INTERFERENCE CANCELLATION SYSTEM

by

Saad Mahboob
Bachelor of Science in Computer Engineering,
COMSATS Institute of Information Technology, Islamabad, 2005

THESIS SUBMITTED IN PARTIAL FULFILLMENT OF
THE REQUIREMENTS FOR THE DEGREE OF

MASTER OF APPLIED SCIENCE

In the
School of Engineering Science

SIMON FRASER UNIVERSITY
Fall 2009

APPROVAL

Name: **Saad Mahboob**

Degree: **Master of Applied Science**

Title of Thesis: **Interference Cancellation System**

Examining Committee:

Chair: **Dr. Carlo Menon**
Assistant Professor of School of Engineering Science

Dr. Shawn Stapleton
Senior Supervisor
Professor of School of Engineering Science

Dr. Rodney Vaughan
Supervisor
Professor of School of Engineering Science

Dr. Sami Muhaidat
Examiner
Assistant Professor of School of Engineering Science

Date Defended/Approved: October 20, 2009

Declaration of
Partial Copyright Licence

ABSTRACT

This thesis examines the problem of coupling of on-channel repeaters in a 3G wireless system. Unwanted feedback occurs between the donor and coverage antennas of a repeater. The unwanted feedback appears as radio echoes which creates interference in the incoming signal from the base station. The thesis describes an adaptive method to suppress these radio echoes. The proposed interference cancellation system (ICS) can detect and cancel the radio echoes from either direct coupling or reflections from buildings around the repeater. A novel multiple-tap radio echo suppressor (RES) is developed and fabricated on the Xilinx Virtex-4 FPGA platform.

Keywords: Repeater, ICS, RES, FPGA

DEDICATION

To my parents

ACKNOWLEDGEMENTS

I wish to thank my loving parents for the encouragement and support in my graduate studies. I am grateful to Professor Shawn Stapleton for giving me an opportunity to study in this prestigious school and financing me during the course of graduate studies. Without his guidance and persistent help, this dissertation would not have been possible.

I am deeply grateful to all the members of my examining committee. I like to thank my colleagues in the Mobile Communication Laboratory for their support. My deepest thanks to Jane and Naeem for reviewing this thesis. Special thanks to Jinyun, Maryam, Alireza, Zeeshan and Arshad. I am also thankful to the administrative staff of the School of Engineering Science and in particular to Raj for her kindness. I also like to thank the library staff of the Simon Fraser University for arranging a useful workshop on thesis preparation.

TABLE OF CONTENTS

LIST OF FIGURES

LIST OF TABLES

LIST OF ABBREVIATIONS

3G	Third Generation
SFN	Single Frequency Network
BS	Base Station
ISI	Intersymbol Interference
AWGN	Additive White Gaussian Noise
DSP	Digital Signal Processing
LOS	Line of Sight
ICS	Interference Cancellation System
RES	Radio Echo Suppressor
MSE	Mean Square Error
MMSE	Minimum Mean Square Error
EVM	Error Vector Magnitude
RCE	Receiver Constellation Error
LMS	Least Mean Square
PDP	Power Delay Profile
SNR	Signal to Noise Ratio
SDA	Steepest Descent Algorithm
dBm	Decibel milliwatt
dBc	Decibel cancellation

PSD	Power Spectral Density
FIR	Finite Impulse Response
Hz	Hertz
FFT	Fast Fourier Transformation
WCDMA	Wideband Code Division Multiple Access
OFDM	Orthogonal Frequency Division Multiplexing
ADC	Analog to Digital Converter
DAC	Digital to Analog Converter
DCM	Digital Clock Manager
IF	Intermediate Frequency
RF	Radio Frequency
LO	Local Oscillator
DDC	Digital Down Converter
DUC	Digital Up Converter
FPGA	Field Programmable Gate Array
VHDL	VHSIC (Very High Speed Integrated Circuits) Hardware Descriptive Language
ASCII	American Standard Code for Information Interchange
UCF	User Constraints File
LUT	Look Up Table
MSPS	Mega Symbols Per Second
MBPS	Mega Bits Per Second
ISE	Integrated Software Environment

CHAPTER 1 INTRODUCTION

1.1 Objective

The objective of this thesis is to develop an ICS repeater for a 3G cellular system. In this thesis, the mathematical algorithm for the ICS repeater is developed and its performance is verified with the hardware test bench.

1.2 Motivation

In the recent years, there is a great demand of seamless services in wireless communication systems. The main challenge to fulfil this demand is the service coverage area. The construction of the service coverage for 3G services equivalent to that of conventional 2G services is very difficult [1]. This is because the propagation loss in the 2 GHz band is much larger than that of the 800 MHz band used by 2G systems. The propagation loss is proportional to the square of the frequency as described by 'free-space path loss formula'. As a result, a large capital investment is required when all the service areas are covered by the base stations [1].

One of the candidates to cover the service area with a low capital investment, especially in the initial stage of a new service introduction is a repeater that relays (repeats) the radio signals between the base station (BS) and the mobile station. Although the repeaters have been used for indoor service coverage such as inside buildings and tunnels, very few repeaters have been

employed for use in open areas because of the radio echoes that occur when the transmit and receive antennas are located close to each other. To use the repeaters successfully in all types of geographical areas, it is necessary to cancel these radio echoes.

In an ICS repeater, the input and output signals are correlated to find the error signal. The adaptive filter uses this error signal to estimate the gain of the channel. Then an anti-phase signal is generated in order to cancel the feedback interference signal. As a result, the echoes are cancelled and the desired output signal is achieved. The ICS repeater can meet the increasing demand for improved isolation between the transmit and receive antennas in complex outdoor wireless environments.

1.3 Accomplishments

The accomplishments of this thesis include:

- Development of the mathematical algorithm for the ICS repeater.
- Simulation of the ICS repeater in MATLAB .
- Implementation of the ICS on a Virtex-4 FPGA and measurement of echo cancellation performance.

1.4 Organization of Thesis

The thesis is organized as follows:

- Chapter 2 gives a literature review about different coupling cancellation systems.
- Chapter 3 describes the ICS algorithm. Simulation results are presented and suppression performance is evaluated.

- Chapter 4 describes briefly the working of the radio echo searcher.
- Chapter 5 discusses the FPGA implementation of the ICS algorithm.
- Chapter 6 concludes the thesis and suggests other directions in this area of research.

CHAPTER 2 BACKGROUND

2.1 Introduction

This chapter gives an overview of the repeater terminology followed by the problem of coupling in the cellular repeaters. Afterwards, common coupling cancellation techniques found in the literature are discussed. The coupling channel model and channel delay spread succeed this.

2.2 Overview

A repeater is used to extend the coverage area of a base station in the cellular network. Coverage extension is used if strength of the received signal is insufficient in a certain area, and the repeater is then used as an additional transmitter often as a part of single frequency network (SFN). Repeaters are a low cost alternative to base stations because they do not require any modulation and demodulation setup or the network equipment used in typical base stations [1]. Cellular repeaters are also known as gap-fillers or relay stations.

A repeater consists of two antennas and a power amplifier. The antennas are identified as donor (receive) and coverage (transmit or service or sector) antennas. The two antennas are typically mounted on the same tower and are located in close proximity. The donor antenna at the repeater is adjusted to be in line of sight (LOS) transmission with the BS. A repeater that receives and transmits signals on the same frequency band is termed as an on-frequency

repeater or SFN repeater [3]. Figure 2.1 shows a general adaptive interference cancellation repeater and the terms associated with it.

Figure 2.1 General adaptive interference cancellation repeater

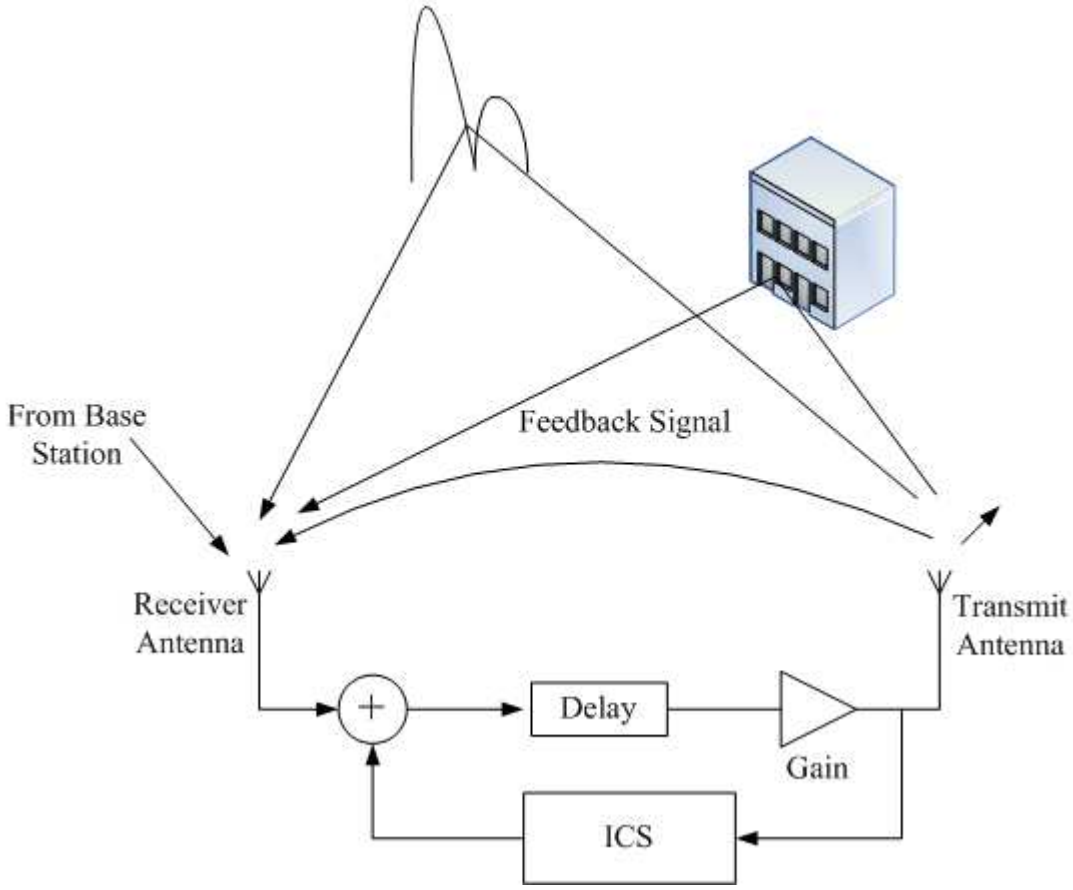

2.3 Coupling between Donor and Service Antennas

When an outdoor repeater is installed, radio echoes are generated between the donor and coverage antennas. These radio echoes act as a source of interference at the donor antenna.

Generally, a repeater with a gain of α dB should have a coupling level sufficiently smaller than $-\alpha$ dB [1] to maintain the repeater stable. Coupling

between the antennas of the repeater approaching $-\alpha$ dB means that significant radio echoes are generated. These echoes can disable the normal operation of the repeater [1].

2.4 Common Techniques of Coupling Interference Cancellation

Traditionally, in order to reduce the coupling, antennas of the repeater are spatially separated or the gain of the repeater is decreased [1,3,4]. However, zoning restrictions for the towers limit the maximum amount of vertical separation that can be realized. Reducing the repeater gain will limit the coverage area. Another way to solve this problem is to use an adaptive cancellation technique that tracks the time-varying coupling channel and generates a correction signal. Adaptive cancellation methods can be used to compensate for the lack of sufficient antenna isolation. Some existing adaptive cancellation algorithms work in the frequency domain, using the reference tones carried in the OFDM signal. Other algorithms use the time domain methods like the LMS. A brief overview of these algorithms is described in this section and their performance and limitations are discussed.

2.4.1 Frequency Domain Interference Cancellation Algorithm

This algorithm is described in [2]. In order to reduce the coupling level between the transmit and receive antennas, the canceller uses a frequency-domain adaptive cancellation method. The transfer function of the coupling path is calculated using the scattered pilot carriers that are contained in the QAM-OFDM signal. Figure 2.2 shows the model given in [2].

Figure 2.2 Frequency domain adaptive ICS

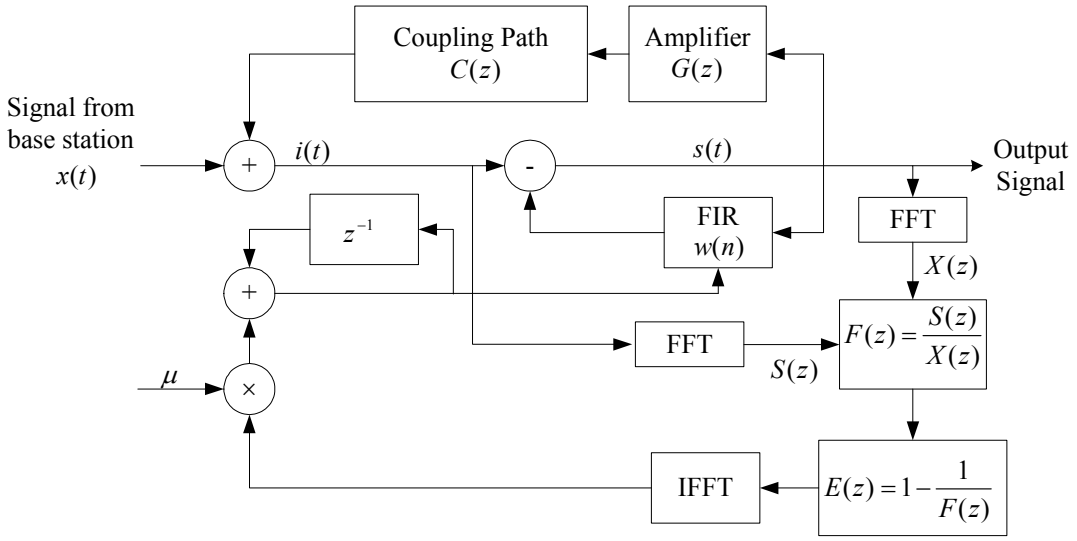

Let the known transmitted signal be $x(t)$. The z-transform of the coupling path is $C(z)$ and that of the relay gain is $G(z)$. The z-transform of the transmitted signal is $X(z)$. From Figure 2.2,

$$I(z) = S(z)G(z)C(z) + X(z) \tag{2.1}$$

and,

$$S(z) = I(z) - S(z)W(z) \tag{2.2}$$

From Equation (2.1) and Equation (2.2),

$$\begin{aligned} S(z) &= \frac{X(z)}{1-\{G(z)C(z)-W(z)\}} \\ &= \frac{X(z)}{1-E(z)} \end{aligned}$$

where z-transform of the error signal is defined as,

$$E(z) = G(z)C(z) - W(z)$$

The coupling signal will be cancelled when the error is zero and,

$$G(z)\ C(z) = W(z)$$

The transfer function of the entire system is,

$$F(z) = \frac{S(z)}{X(z)} = \frac{1}{1 - E(z)} \tag{2.3}$$

The FFT algorithm is used to calculate $S(z)$ and $X(z)$. From Equation (2.3), the z-transform of the error signal is described in terms of the system transfer function $F(z)$ as,

$$E(z) = 1 - \frac{1}{F(z)}$$

The time domain error $e(n)$ is calculated by taking the inverse Fourier transformation of the error transfer function,

$$e(n) = IFT\left[1 - \frac{1}{F(z)}\right]$$

The error signal $e(n)$ is used to update the channel gain estimate $w(n)$ using the relation,

$$w(n) = w(n-1) + \mu\, e(n)$$

where μ is the step-size. Sequential updating of the channel coefficient $w(n)$ allows the channel tracking to be performed. Due to the need for OFDM demodulation and frequency response estimation using the FFT, the computational complexity of this algorithm is generally high, which limits the usability of this algorithm.

2.4.2 LMS Adaptive Interference Cancellation Algorithm

This algorithm is described in [4]. It explains the LMS approach to reduce the coupling. This algorithm does not require pilot symbols for the channel

estimation process and suppresses the coupling using the minimum output power criterion. Experimental results verify that this algorithm works well in the fading channels. The tracking ability of the LMS based interference cancellation algorithm depends upon the length of the adaptive filter; that in turn depends upon the channel delay profile. If the channel has a large delay spread, the interference suppression capability is affected.

The repeater in [4] is regenerative in nature. This implies that after interference cancellation, the repeater extracts the data using some detection algorithm and re-modulates it. This processing introduces a delay of several symbols at the output of the repeater. In [4], the authors show the interference cancellation to be a two stage process i.e., RF stage and baseband stage.

Similarly, [1] introduces an autocorrelation based interference cancellation system that can suppress multiple feedback radio echoes. However, [1] discusses the deployment of ICS in 2G wireless systems and does not discuss the 3G wireless scenario. 3G systems support a higher data rate and a greater carrier bandwidth as opposed to 2G networks. 2G systems use the 900 MHz or 1800 MHz frequency bands whereas 3G systems use the 2100 MHz frequency band. In addition, [1] does not discuss the effect of step-size factor, radio echo Doppler frequency and SNR on the performance of the ICS.

2.5 Feedback Loop Channel Model

In this thesis, the channel between the base station and repeater is assumed to be line of sight (LOS) AWGN channel. The channel between the

donor and coverage antennas is modeled as a frequency selective Rayleigh fading channel. It can be represented by the following complex valued low-pass impulse response [7],

$$h(t) = \sum_{l=1}^{P-1} a_l(t)\ e^{-j\theta_l(t)}\ \delta(t-\tau_l)$$

where $\delta(\cdot)$ is the Dirac delta function, l is the channel index, P is the total number of multipath components of the channel, $a_l(t)e^{-j\theta_l(t)}$ are the time dependent channel coefficients which are usually complex Gaussian distributed and τ_l is the delay between the input and the l^{th} tap. The channel coefficients (also termed as channel taps or path gains) are independent and identically distributed. Typically, the channel taps decay according to an exponential profile with each tap having an independent fading coefficient [7]. The amplitudes $a_l(t)$ follow a Rayleigh distribution whereas the phases $\theta_l(t)$ follow a uniform distribution. The channel between the repeater antennas is assumed as quasi-static. This implies that the path gains change insignificantly over a period of $\frac{1}{F_D}$, where F_D corresponds to the maximum radio echo Doppler frequency. Since this period corresponds to a very large number of bits, assessing the performance of the repeater over a significant range of fading requires a long simulation time [13].

2.6 Channel Delay Spread

The delay spread determines the delay characteristics of the multipath channel. If the delay spread is smaller than the symbol duration, then the channel is termed as a flat fading channel and can be modeled as a single path. In other words, the bandwidth of the signal is small compared to the bandwidth of the fading channel. The channel has a flat spectrum across the signal bandwidth and it does not alter the frequency characteristics of the signal. As a result, there is no intersymbol interference (ISI).

If the delay profile of the channel is greater than the symbol duration, then frequency selective fading occurs. The channel no longer has a flat spectrum across the bandwidth of the signal and different parts of the signal spectrum encounter different channel frequency response. The bandwidth of the signal is greater than the bandwidth of the fading channel. As a result, there will be ISI in the system.

Usually, power delay profile (PDP) is considered as a useful tool to obtain knowledge about the strength and delay characteristics of the multipath components of the channel [3]. PDP of the coupling channel for 1.823 GHz on-frequency repeater is shown in Figure 2.3. In Figure 2.3, the strongest component is normalized to 0 dB. The horizontal bar in the figure represents the system noise floor [3]. In Figure 2.3, several strong multipath signals are distributed throughout the PDP, mostly within the first 1.5 μs . These multipath signals are most likely caused by reflections from the large signboards and buildings near the repeater. Weak peaks in the PDP are caused by reflections

from the vehicular traffic [3]. Usually, the delay spread of the coupling channel varies from 0.11 μs to 6.22 μs [8].

Figure 2.3 Sample PDP from a measurement site. Reproduced from [3]

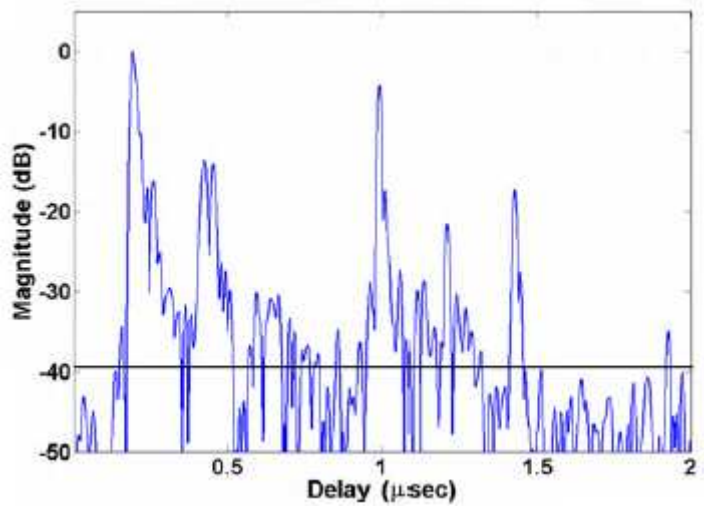

2.7 Learning Curve and Mean Square Error

A curve obtained by plotting the mean square error (MSE) of the adaptive filter versus the iteration index l is termed as "learning curve". Learning curve can help to understand the performance of the adaptive filter, including the convergence speed, steady state error and stability. MSE is defined as the ensemble average of the squared absolute error between the ideal and estimated channel gains. It is mathematically expressed as,

$$MSE = E\left\{\left|w + M_l\right|^2\right\}$$

where w and M_l are the ideal and estimated channel gains respectively, and E is the ensemble average operator. The ensemble average is calculated by

averaging the MSE over a number of independent trials. Further details about the MSE are given in Appendix 1.

2.8 ICS for 3G Wireless Systems

The ICS repeater discussed in this thesis is developed for 3G wireless system. The use of ICS repeaters for the 3G technology is not discussed in the literature so far. 3G networks using a WCDMA signal have a bandwidth of 5 MHz and a data rate of 3.84 MSPS [14].

2.9 Summary

This chapter has covered different aspects related to the wireless repeaters. The main items covered in this chapter are:

- Overview of the repeater systems.
- Coupling and the problem it creates.
- Techniques proposed in the literature to mitigate coupling.
- Mathematical model of the coupling path.
- Channel delay profile.
- Learning curve and mean square error.

CHAPTER 3 RADIO ECHO SUPPRESSOR

3.1 Introduction

This chapter presents an interference cancellation system (ICS) based on the steepest descent algorithm (SDA) that can blindly cancel the coupling radio echoes and makes use of the second order statistics i.e., correlation [9,11] to produce an error signal. The proposed ICS algorithm has a low complexity and it does not require any training sequence or pilot symbols for the channel estimation. The algorithm works well in an environment with deep fades between the donor and coverage antennas. This chapter describes the ICS algorithm and explains its various characteristic features using the MATLAB simulations.

3.2 System Model and Algorithm Description

The path between the antennas of a repeater includes a combiner, a de-correlation delay τ and a power amplifier (gain of the repeater). The delay τ is used to insure that the signals transmitted from the BS are uncorrelated with the feedback radio echoes. The signal from output of the repeater $C(n)$ is delayed to match the delay of the radio echo $U_a(t)$, where the subscript a denotes the analog signal. Correlation is used in the radio echo suppressor to generate the error signal Λ_l [1]. A step-size μ is multiplied with the error signal Λ_l and accumulated to create the estimated channel coefficient M_l. The estimated channel gain is multiplexed with the delayed version of the signal $C(n)$ to

generate the suppression signal $S(n)$. The suppression signal is added to the incoming signal $R(n)$ to cancel the interference. Figure 3.1 shows the block diagram of a single-tap correlation based RES.

Figure 3.1 Block diagram of single-tap RES

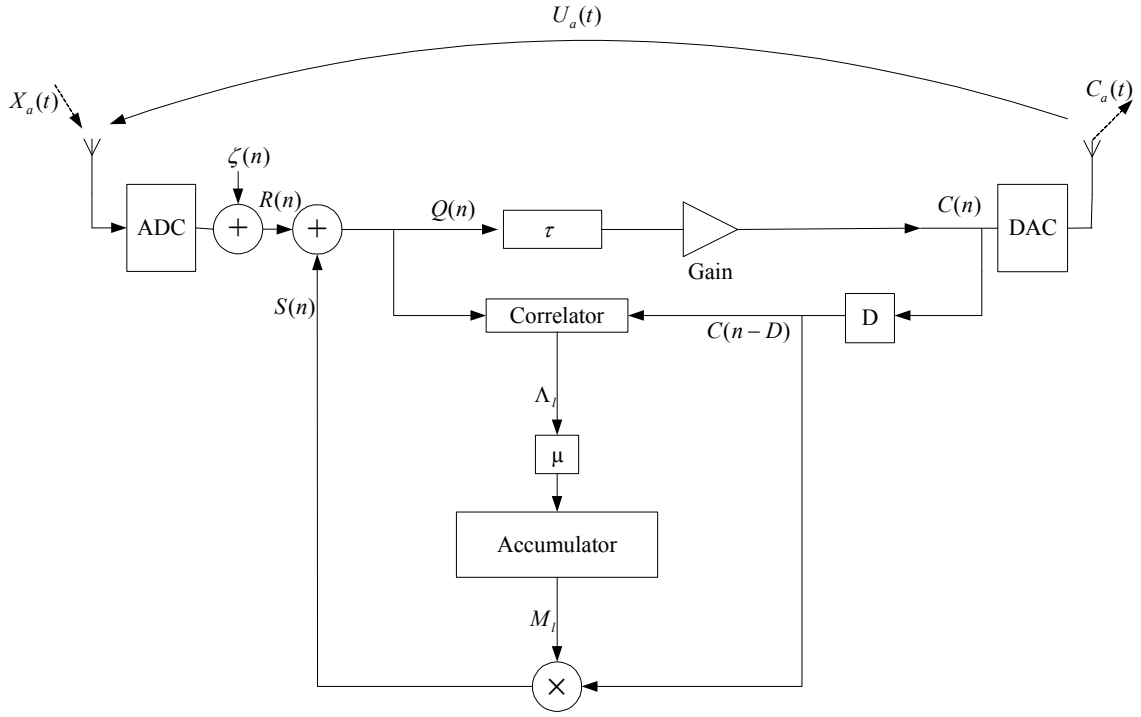

Since discrete time processing is used, n is used instead of t . l is used as an iteration index. For simplification, the gain of the repeater is set to unity. The transmitted signal from the base station $X_a(t)$ and the coupling signal $U_a(t)$ are received at the repeater as,

$$R(n) = X(n) + U(n)$$

where,

$$U(n) = U_a(nT_s) \qquad -\infty < n < \infty$$

and

$$X(n) = X_a(nT_s) \qquad -\infty < n < \infty$$

are the discrete time counterparts of $U_a(t)$ and $X_a(t)$ respectively, and T_s refers to the sampling time. Radio echo $U(n)$ is a delayed and attenuated version of the output signal $C(n)$. $U(n)$ can be expressed as,

$$\begin{aligned} U(n) &= w_l\, C(n-k) \\ &= w_l\, Q(n-\tau-k) \end{aligned}$$

where $k = D$ is a positive integer that denotes the time shift that results in a delay of the signal by D units of time. In this thesis, we assume the radio echo delay D to be integer multiple of the sampling time. w_l is the complex channel gain at the iteration l. τ is chosen to be much greater than the symbol period T_{symbol} i.e. $\tau >> T_{symbol}$,to insure that the signals $X(n)$ and $C(n)$ are uncorrelated with each other. τ is defined as,

$$\tau = N_o\, T_s$$

where N_o is a positive integer. When the suppression signal $S(n)$ is added to the received signal $R(n)$, which contains the interference, the residual component (also called system error) $\varepsilon_{system}(n)$ is produced and is expressed as,

$$\varepsilon_{system}(n) = U(n) + S(n)$$

After the signals $S(n)$ and $R(n)$ are added together, the signal used for the correlation is [1],

$$\begin{aligned} Q(n) &= R(n) + S(n) \\ &= X(n) + \varepsilon_{system}(n) \end{aligned}$$

3.3 Cost Function

As the interference signal $U(n)$ is cancelled by the suppression signal $S(n)$, the power of the error signal $\varepsilon_{system}(n)$ decreases. In this thesis, the average energy of the signal $Q(n)$ is taken as the cost function and is optimized.

$$\begin{aligned} J_l &= E\left[\left|Q(n)\right|^2\right] \\ &= E\left[\left|R(n)+S(n)\right|^2\right] \\ &= E\left[\left|R(n)+M_l\,C(n-D)\right|^2\right] \\ &= E\left[\left|X(n)+U(n)+\zeta(n)+M_l\,C(n-D)\right|^2\right] \\ &= E\left[\left|X(n)+w_l\,C(n-D)+\zeta(n)+M_l\,C(n-D)\right|^2\right] \end{aligned} \tag{3.1}$$

where in Equation (3.1), E denotes the statistical average operator, M_l denotes the suppression coefficient which represents an estimate of the channel gain w_l at the lth iteration, J_l represents the value of the cost function at the iteration l and $\zeta(n)$ is the AWGN noise component.

$$\begin{aligned} &= E\left[\left|X(n)+w_lC(n-D)+M_lC(n-D)\right|^2+\left|\zeta(n)\right|^2\right] \\ &\quad + E\left[2\left|X(n)+w_lC(n-D)+M_lC(n-D)\right|\left|\zeta(n)\right|\right] \\ &= E\left[\left|X(n)+w_lC(n-D)+M_lC(n-D)\right|^2+\left|\zeta(n)\right|^2\right] \\ &\quad + \left[2E\left|X(n)\zeta(n)\right|+E\left|w_lC(n-D)\zeta(n)\right|+E\left|M_lC(n-D)\zeta(n)\right|\right] \\ &= E\left[\left|X(n)+w_lC(n-D)+M_lC(n-D)\right|^2+\left|\zeta(n)\right|^2\right] \\ &\quad + \left[2\,E\left|X(n)\right|E\left|\zeta(n)\right|+w_l\,E\left|C(n-D)\right|E\left|\zeta(n)\right|+M_l\,E\left|C(n-D)\right|E\left|\zeta(n)\right|\right] \end{aligned}$$

where the signals $X(n)$ and $C(n-D)$ are assumed to be independent of $\zeta(n)$. Since the incoming signal $X(n)$ and noise $\zeta(n)$ have a zero mean, so $E\left[X(n)\right]=0$, $E\left[C(n-D)\right]=0$ and $E\left[\zeta(n)\right]=0$, and we are left with,

$$J_l = E\left[\left|X(n)+w_lC(n-D)+M_lC(n-D)\right|^2+\left|\zeta(n)\right|^2\right]$$

$$
\begin{aligned}
&= E\left[\left|X(n)+\{w_l+M_l\}C(n-D)\right|^2+\left|\zeta(n)\right|^2\right] \\
&= E\left[\left|X(n)+\{w_l+M_l\}C(n-D)\right|^2\right]+E\left[\left|\zeta(n)\right|^2\right] \\
&= \sigma_X^2+\left|w+M_l\right|^2\sigma_C^2+2\left|w+M_l\right|E\left\{\left|X(n)C(n-D)\right|\right\}+\sigma_\zeta^2 \\
&= \sigma_X^2+\left|w_l+M_l\right|^2\sigma_C^2+2\left|w+M_l\right|\Re[\psi]+\sigma_\zeta^2
\end{aligned}
$$

where $\Re[\psi]$ denotes the correlation between the signals $X(n)$ and $C(n-D)$, σ_X^2 denotes the variance of the incoming signal from the BS $X(n)$ and σ_ζ^2 represents the variance of the noise $\zeta(n)$. $\Re[\psi]$ has a very small value, since the signals $X(n)$ and $C(n-D)$ are uncorrelated because of chosen delay τ. Finally,

$$
J_l = \sigma_X^2+\sigma_\zeta^2+\left|w_l+M_l\right|^2\sigma_C^2 \tag{3.2}
$$

Equation (3.2) shows that the cost function has an optimum value w_o when,

$$
M_l = -w_o
$$

where w_o is the value of w_l that gives the minimum value of cost function. The resulting minimum mean square error (MMSE) that represents the minimum value of the cost function $J_{\min}$ will be,

$$
J_{\min} = MMSE = \sigma_X^2+\sigma_\zeta^2
$$

3.4 Steepest Descent Algorithm

The steepest descent algorithm (SDA) (also called gradient descent algorithm) is an iterative technique used to approximate an optimum value of the cost function. To find the minimum value of a function, the steepest descent algorithm takes steps proportional to the negative of the gradient of the cost function at the current point [18].

Given the cost function J and without any knowledge about its minimum, the steepest descent algorithm starts with an initial guess for M_l, and then improves the guess in a recursive manner until the optimum value $M_l = -w_o$ is reached. The procedure that SDA follows is of the form,

New estimate = Old estimate + Correction term

or more explicitly,

$$M_l = M_{l-1} + \mu\rho, \quad l \geq 1 \tag{3.3}$$

where M_{l-1} denotes the channel gain estimate at the iteration $(l-1)$ and M_l denotes the updated channel gain estimate at the iteration l. The correction term is a product of a scalar μ (called step-size) and a factor ρ. ρ is an error function i.e., $\rho = f(error)$ where $f(\cdot)$ denotes the function. The product $\mu\rho$ then defines the direction in which the current estimate is to be corrected for guaranteed convergence. The step-size μ determines how small or large the correction term will be and is a negative constant. μ and ρ are selected to enforce the condition $J(M_l) < J(M_{l-1})$. In this way, the value of the cost function at successive iterations will be monotonically decreasing until the estimate reaches the optimum value. The features of the steepest descent algorithm are as follows:

(1) It converges and fluctuates about w_o.

(2) The gradient estimate is noisy.

(3) The update steps are random.

(4) $\lim_{l\to\infty} E\{M_l\} = w_o$

3.5 Adaptive Algorithm

The signal used to create the suppression signal is,

$$C(n) = X(n-\tau) + \varepsilon_{system}(n-\tau)$$

This signal is passed through the delay D to get a delayed signal,

$$C(n-D) = X(n-\tau-D) + \varepsilon_{system}(n-\tau-D)$$

In the ICS repeater, the complex signal samples $Q(n)$ and $C(n-D)$ are correlated to generate the correlation error signal $e_l(n)$.

$$\begin{aligned}
e_l(n) &= Q(n)\ C(n-D)^* \\
&= \left[X(n) + \varepsilon_{system}(n)\right]\left[X(n-\tau-D) + \varepsilon_{system}(n-\tau-D)\right]^* \\
&= X(n)\left[X(n-\tau-D) + \varepsilon_{system}(n-\tau-D)\right]^* + \varepsilon_{system}(n) \\
&\quad \left[X(n-\tau-D) + \varepsilon_{system}(n-\tau-D)\right]^* \\
&= X(n)\ X(n-\tau-D)^* + X(n)\ \varepsilon_{system}(n-\tau-D)^* + \varepsilon_{system}(n)\ X(n-\tau-D)^* \\
&\quad + \varepsilon_{system}(n)\ \varepsilon_{system}(n-\tau-D)^*
\end{aligned}$$

Because of the de-correlation delay τ, the correlation between $X(n)$ and $X(n-\tau-D)$ is very small and can be ignored.

$$\begin{aligned}
e_l(n) = X(n)\ \varepsilon_{system}(n-\tau-D)^* + \varepsilon_{system}(n)\ X(n-\tau-D)^* + \\
\varepsilon_{system}(n)\ \varepsilon_{system}(n-\tau-D)^*
\end{aligned} \tag{3.4}$$

To simplify Equation (3.4) further, the residual component $\varepsilon_{system}(n)$ is expressed as a function of $X(n)$ as,

$$\begin{aligned}
\varepsilon_{system}(n) &= U(n) + S(n) \\
&= w_l\ C(n-D) + M_l\ C(n-D) \\
&= w_l\ \left[X(n-\tau-D) + \varepsilon_{system}(n-\tau-D)\right] + M_l \\
&\quad \left[X(n-\tau-D) + \varepsilon_{system}(n-\tau-D)\right] \\
&= f\left(X(n)\right)
\end{aligned}$$

Since $\varepsilon_{system}(n)$ is a function of $X(n)$, this implies that $\varepsilon_{system}(n-\tau-D)^*$ is also a function of $X(n-\tau-D)$. Hence $X(n)\,\varepsilon_{system}(n-\tau-D)$ and $\varepsilon_{system}(n)\,X(n-\tau-D)^*$ in Equation (3.4) are approximately equal to zero. Finally, Equation (3.4) simplifies to,

$$
\begin{aligned}
e_l(n) &= \varepsilon_{system}(n)\;\varepsilon_{system}(n-\tau-D)^* \qquad (3.5)\\
&= \{U(n)+S(n)\}\;\varepsilon_{system}(n-\tau-D)^*\\
&= \{w_l\,C(n-D)+M_l\,C(n-D)\}\;\varepsilon_{system}(n-\tau-D)^*\\
&= \{w_l+M_l\}C(n-D)\;\varepsilon_{system}(n-\tau-D)^*\\
&= \{w_l+M_l\}C(n-D)\;\{C(n-D)-X(n-\tau-D)\}^*\\
&= \{w_l+M_l\}|C(n-D)|^2\\
&= \{w_l+M_l\}|Q(n-\tau-D)|^2 \qquad (3.6)
\end{aligned}
$$

Equation (3.5) shows that the correlation error $e_l(n)$ depends upon the correlation of the residual terms $\varepsilon_{system}(n)$ and $\varepsilon_{system}(n-\tau-D)$. Equation (3.5) is integrated over the correlation period N to get the accumulated error.

$$E_l = \sum_{i=0}^{N} e_l(i) \qquad (3.7)$$

The accumulated error given by Equation (3.7) is used in the SDA to update the channel gain estimate. Usually, normalized correlation error Λ_l is used since the accumulated error given by Equation (3.7) can yield a large number. Normalization on the other hand gives a relative value and varies between $+1$ and -1.

$$\Lambda_l = \frac{E_l}{\sqrt{\sum_{i=0}^{N}|Q(i)|^2 \times \sum_{i=0}^{N}|C(i-D)|^2}} \qquad (3.8)$$

Λ_l is used as the error function in the SDA i.e.,

$$\rho = \Lambda_l$$

The recursion given by Equation (3.3) becomes,

$$M_l = M_{l-1} + \mu \Lambda_{l-1} \tag{3.9}$$

The step-size is chosen as a compromise between the speed of convergence and the SNR. In practice, a large step-size yields fast convergence that allows the algorithm to track rapid fluctuations due to fading, at the expense of increased noise in the channel gain estimate. This affects the interference cancellation of the ICS repeater. Similarly, a small value of the step-size makes the convergence of the adaptive algorithm slow.

3.6 Condition on Step-size for Convergence

The reference [1] describes the convergence criterion of an ICS. Substituting the value of $e_l(n)$ from Equation (3.6) into Equation (3.7) and using it in Equation (3.8),

$$\begin{aligned}
\Lambda_l &= \frac{\{w_l + M_l\} \sum_{i=0}^{N} \left| Q(i-\tau-D) \right|^2}{\sqrt{\sum_{i=0}^{N} \left| Q(i) \right|^2 \times \sum_{i=0}^{N} \left| C(i-D) \right|^2}} \\
&= \frac{\{w_l + M_l\} \sum_{i=0}^{N} \left| Q(i-\tau-D) \right|^2}{\sqrt{\sum_{i=0}^{N} \left| Q(i) \right|^2 \times \sum_{i=0}^{N} \left| Q(i-\tau-D) \right|^2}} \\
&= \frac{\{w_l + M_l\} \sqrt{\sum_{i=o}^{N} \left| Q(i-\tau-D) \right|^2}}{\sqrt{\sum_{i=0}^{N} \left| Q(i) \right|^2}} \\
&= K_l \{w_l + M_l\}
\end{aligned} \tag{3.10}$$

where,

$$K_l = \frac{\sqrt{\sum_{i=o}^{N} \left| Q(i-\tau-D) \right|^2}}{\sqrt{\sum_{i=0}^{N} \left| Q(i) \right|^2}}$$

substituting Equation (3.10) in Equation (3.9),

$$\begin{aligned} M_l &= M_{l-1} + \mu \Lambda_{l-1} \\ &= M_{l-1} + \mu K_{l-1} \{ w_{l-1} + M_{l-1} \} \\ &= M_{l-1} + \mu K_{l-1} w_{l-1} + \mu K_{l-1} M_{l-1} \\ &= M_{l-1} [1 + \mu K_{l-1}] + \mu K_{l-1} w_{l-1} \end{aligned}$$

adding a term w_{l-1} to both sides,

$$\begin{aligned} M_l + w_{l-1} &= M_{l-1} [1 + \mu K_{l-1}] + \mu K_{l-1} w_{l-1} + w_{l-1} \\ &= M_{l-1} [1 + \mu K_{l-1}] + w_{l-1} [\mu K_{l-1} + 1] \\ &= [1 + \mu K_{l-1}] [M_{l-1} + w_{l-1}] \\ &= [1 + \mu K_{l-1}][1 + \mu K_{l-2}][M_{l-2} + w_{l-2}] \\ &= \left[\prod_{i=1}^{l-1} (1 + \mu K_i) \right] [M_1 + w_1] \end{aligned} \qquad (3.11)$$

In Equation (3.11), $(1 + \mu K_i) > 0$. Solving it gives,

$$-\frac{1}{K_i} < \mu < 0$$

Therefore if the above condition is fulfilled for all l, then

$$\begin{aligned} &\lim_{l \to \infty} (M_l + w_l) = 0 \\ &\lim_{l \to \infty} M_l = -w_o \end{aligned} \qquad (3.12)$$

Equation (3.12) shows that the cancellation of the radio echo is accomplished by generating a suppression coefficient M_l which has the same magnitude as that of the channel coefficient w_l. However, the angle of M_l is π radian out of phase

to the angle of w_l. In other words, the suppression signal $S(n)$ converges to $-U(n)$ as the ICS works. Further details are given in Appendix 2.

3.7 Multiple Radio Echo Suppressors and Circuit Configuration of ICS

The ICS is usually programmed on a FPGA. Since a single RES is capable of suppressing only one radio echo, in order to suppress several radio echoes simultaneously, several RES circuits are programmed on the same FPGA. This unit is called multiple radio echo suppressor (MRES). In addition, an echo searcher is also used in order to calculate the delay D for each radio echo [1].

The radio echo searcher works in parallel with the MRES but at a much slower rate. If a new radio echo is found in the PDP, the echo searcher informs the controller to take the desired action. The unused radio echo suppressors are used successively starting from an echo with the biggest magnitude. Similarly, the RES is set to an idle state when its contribution in the overall interference cancellation is small. The contribution of the suppressors in the overall interference cancellation is periodically supervised by the controller, by observing the output of the correlator in each RES [1]. Figure 3.2 shows the block diagram of a complete ICS.

Figure 3.2 Complete ICS with MRES and a radio echo searcher

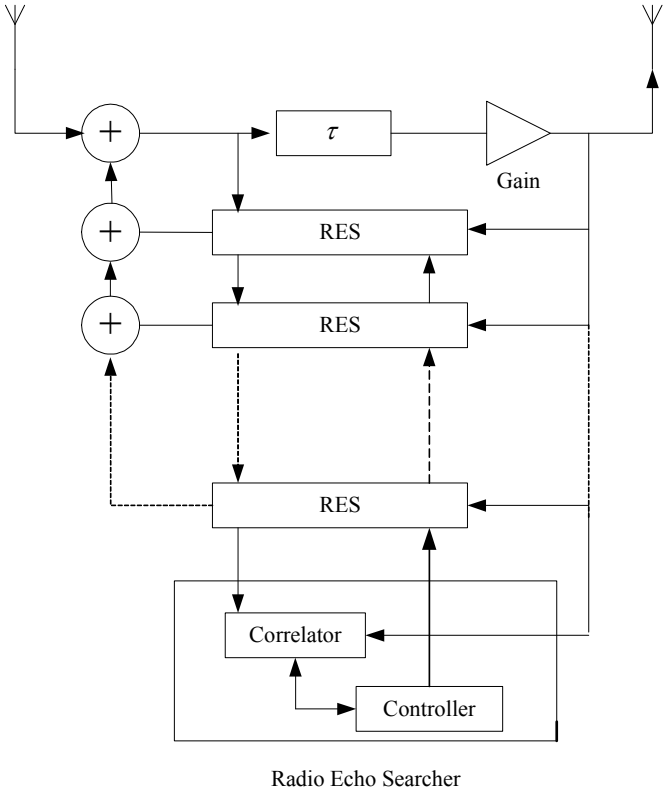

3.8 Error Vector Magnitude

The error vector magnitude (EVM), sometimes also called receive constellation error (RCE), is a measure used to quantify the performance of a digital receiver [15]. EVM is a measure of how far the received symbols are away from the ideal locations in the constellation plot. EVM is a scalar quantity and is mathematically represented as a ratio of power of the error signal to the power of the original signal. By convention, EVM is reported as a percentage.

$$Mean\ \ power\ \ of\ \ error\ signal = \frac{\Sigma \left| Error\ signal \right|^2}{N}$$

$$Mean\ \ power\ \ of\ \ original\ signal = \frac{\Sigma \left| Original\ \ \ signal \right|^2}{N}$$

where N is the number of symbols in the constellation used for EVM calculation.

$$EVM = \sqrt{\frac{Mean\ power\ of\ error\ signal}{Mean\ power\ of\ original\ \ signal}} \times 100\%$$

Figure 3.3 EVM and its components

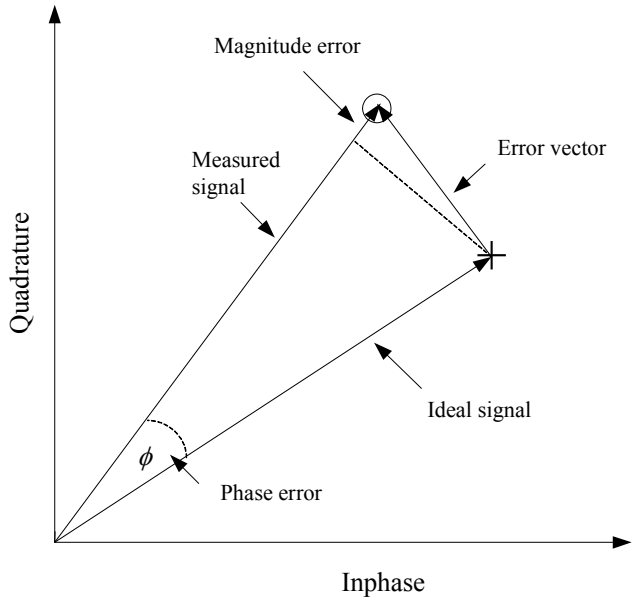

3.9 Simulation Results

Numerous simulations are performed to illustrate different features of the ICS. An ICS repeater with three echo suppressors to suppress three echoes is implemented. In this thesis, our focus is on the frequency selective channel. In a frequency selective channel, the received signal is dispersed due to multiple versions of the transmitted signal, attenuated and delayed in time due to radio echoes. The variance of the transmitted signal from the BS is set to 1 and the radio echo Doppler frequency is set to 10 Hz. The mean value of the three radio

echoes are set to 0.4, 0.3 and 0.2; which correspond to echoes having -8 dB, -10 dB and -14 dB less power than the power of the transmitted signal. The value of the step-size μ is fixed as -0.0001.

Figure 3.4 shows the three radio echo suppressors in the ICS repeater tracking the magnitude components of the respective echoes. It is clear from Figure 3.4 that the ICS works quite well in the deep fading environments.

Figure 3.4 Magnitude tracking ability of three radio echo suppressors

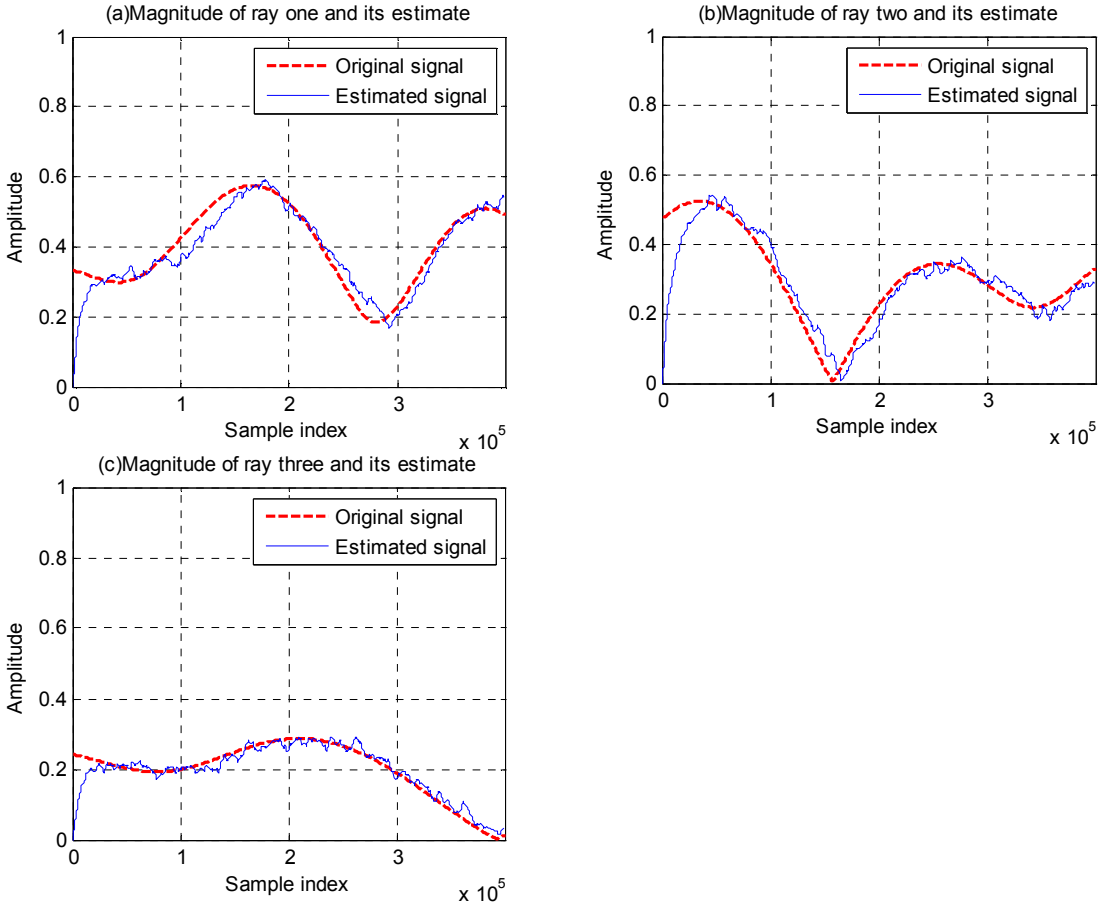

Figure 3.5 gives the phase tracking ability of the three radio echo suppressors discussed in Figure 3.4. It can be seen that in each RES, the suppression coefficient M_l has an angle opposite to the angle of the channel coefficient w_l. The phase plots in Figure 3.5 are unwrapped. The 'unwrap' function in the MATLAB corrects the radian phase angles in the vector passed to it as an argument by adding multiples of $\pm 2\pi$ radian to remove the absolute jumps greater than π radian between the consecutive values [MATLAB®]. Figure 3.6 gives the result when the phases of the suppression coefficient and channel coefficient are added together. The resultant phase is a straight line representing either π or $-\pi$ radians.

Figure 3.5 Phase tracking ability of three radio echo suppressors

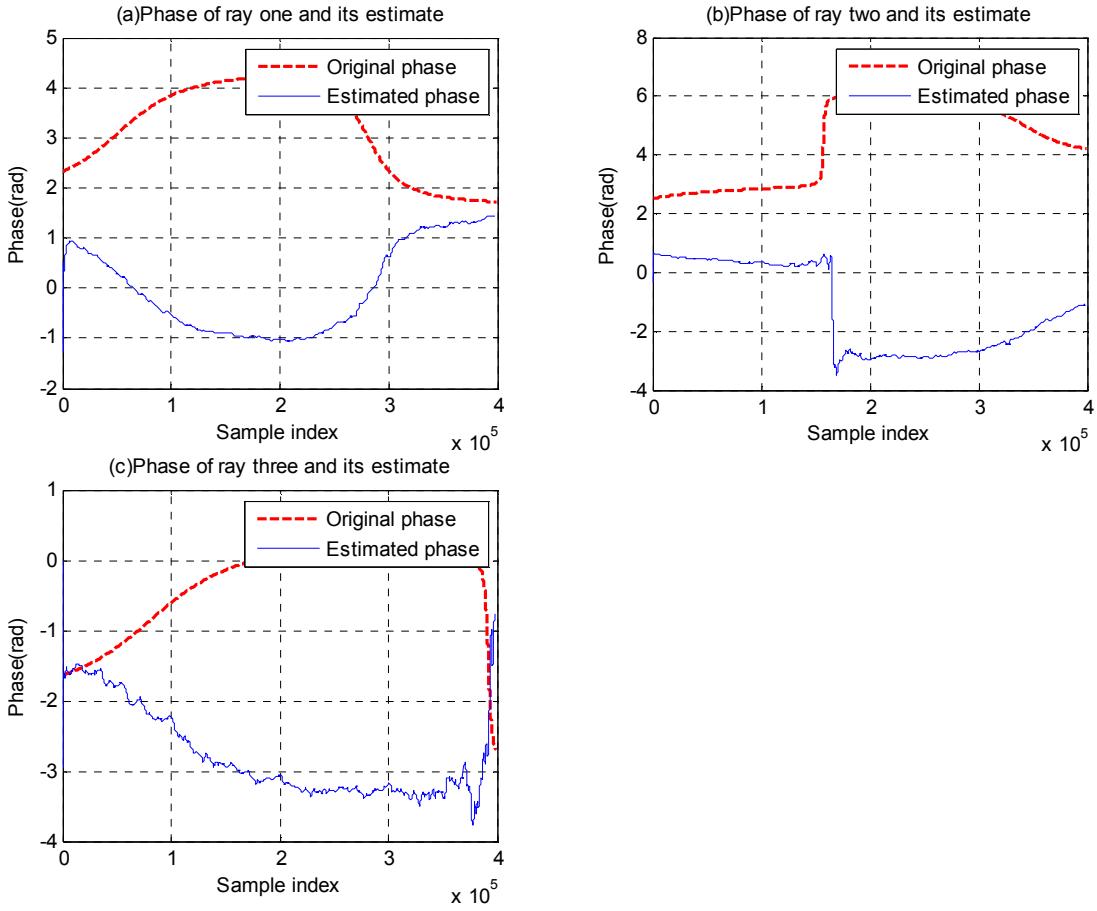

Figure 3.6 Phase components of suppression coefficient and channel coefficient added

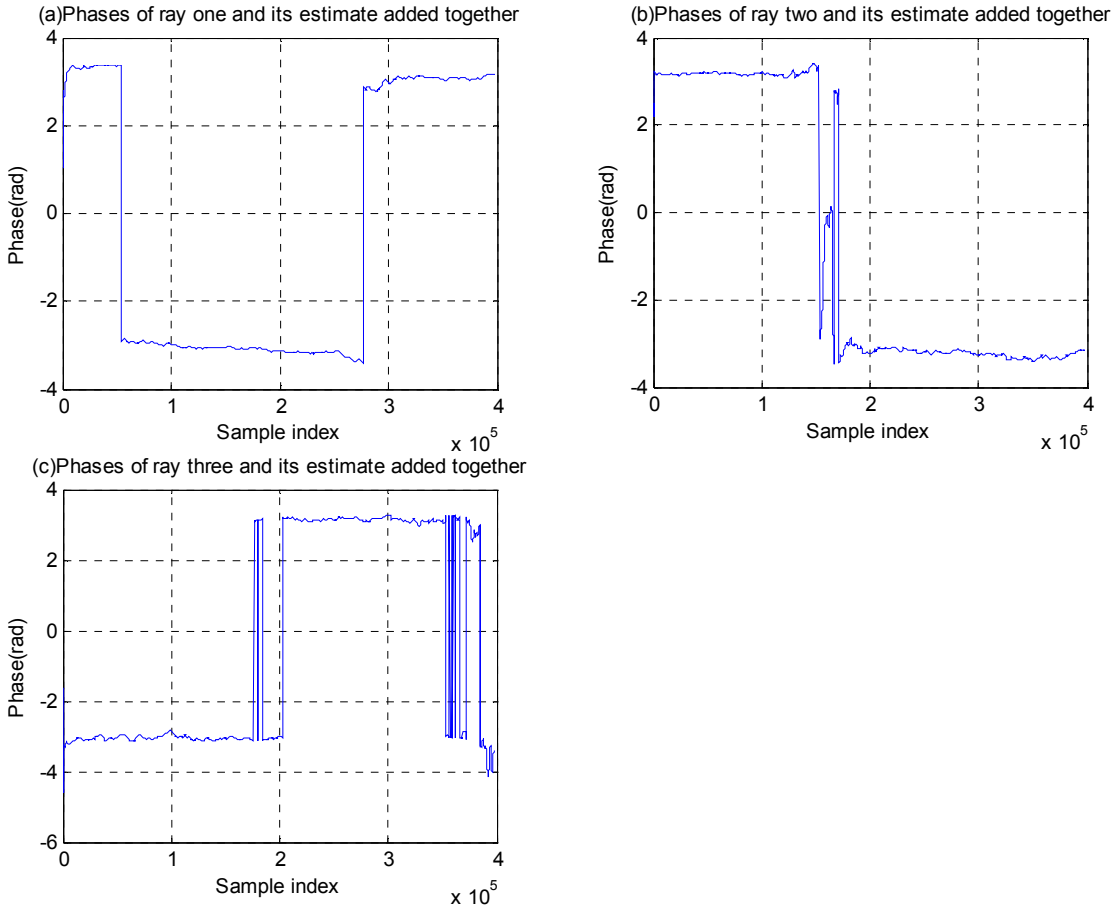

Figure 3.7 shows the learning curve of the ICS repeater. It is observed from Figure 3.7 that on average 25000 iterations are required for the system to converge to a steady state. The system is said to have reached a steady state when the MSE is below a certain threshold. Since the sampling time is $10.851 ns$, the convergence time of the ICS is,

Convergence time = Number of iterations to converge x sampling time
= 25000 x 10.851 ns
=0.271 ms

Figure 3.7 Ensemble averaged learning curve of ICS for Fd =10 Hz

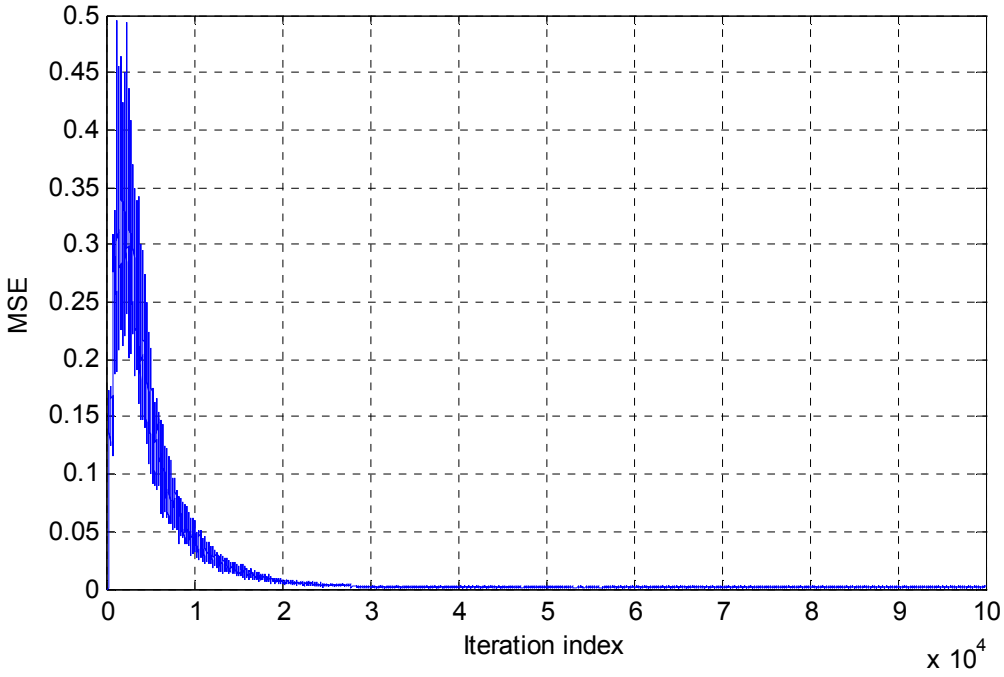

The interference cancellation ability of the ICS is presented through the spectral plots. Figures 3.8(a) and (b) show the spectrums of the transmitted signal and interference signal respectively. Figure 3.8(d) displays the spectrum of the suppression signal. Figure 3.8(c) shows the spectrum of the signal at the output of the ICS when it is working. Table 3.1 gives the averaged power spectral density (PSD) values of various signals. In Table 3.1, the cancellation ability of the ICS is determined by taking the absolute value of the difference between the average PSD value of the interference signal and the average PSD value of the error signal. The unit of interference cancellation is decibel cancellation (dBc).

Figure 3.8 Spectrum of various signals in ICS

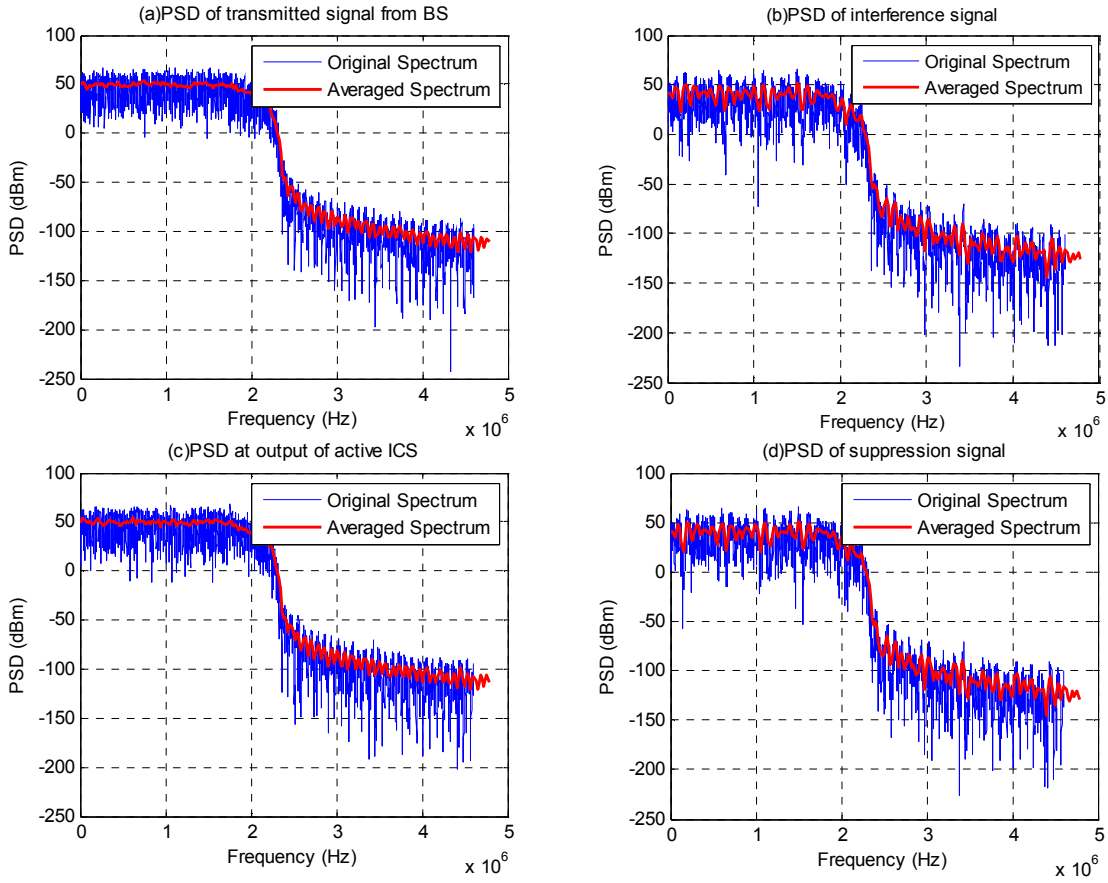

Table 3.1 Average PSD of different signals in ICS

Signal	Average PSD value
Transmitted signal from BS	49.13 dBm
Interference signal	40.16 dBm
Output signal	49.92 dBm
Error signal	0.43 dBm
Suppression signal	39.72 dBm
Cancellation relative to interference	39.73 dBc

Figure 3.9(a) is the constellation diagram of the WCDMA signal transmitted from the base station and corrupted by AWGN noise. The SNR of this signal is 25 dB and its EVM is 7.6%. Figure 3.9(b) shows the constellation of the signal at output of the ICS repeater when it is turned off. The EVM of this signal is 36.67%. The constellation of the output signal when the ICS is active is shown in Figure 3.9(c) and its EVM is calculated to be 10.04%, well within the 17.5% maximum allowed EVM for a UMTS repeater [3].

Figure 3.9 Constellation plots before and after interference cancellation

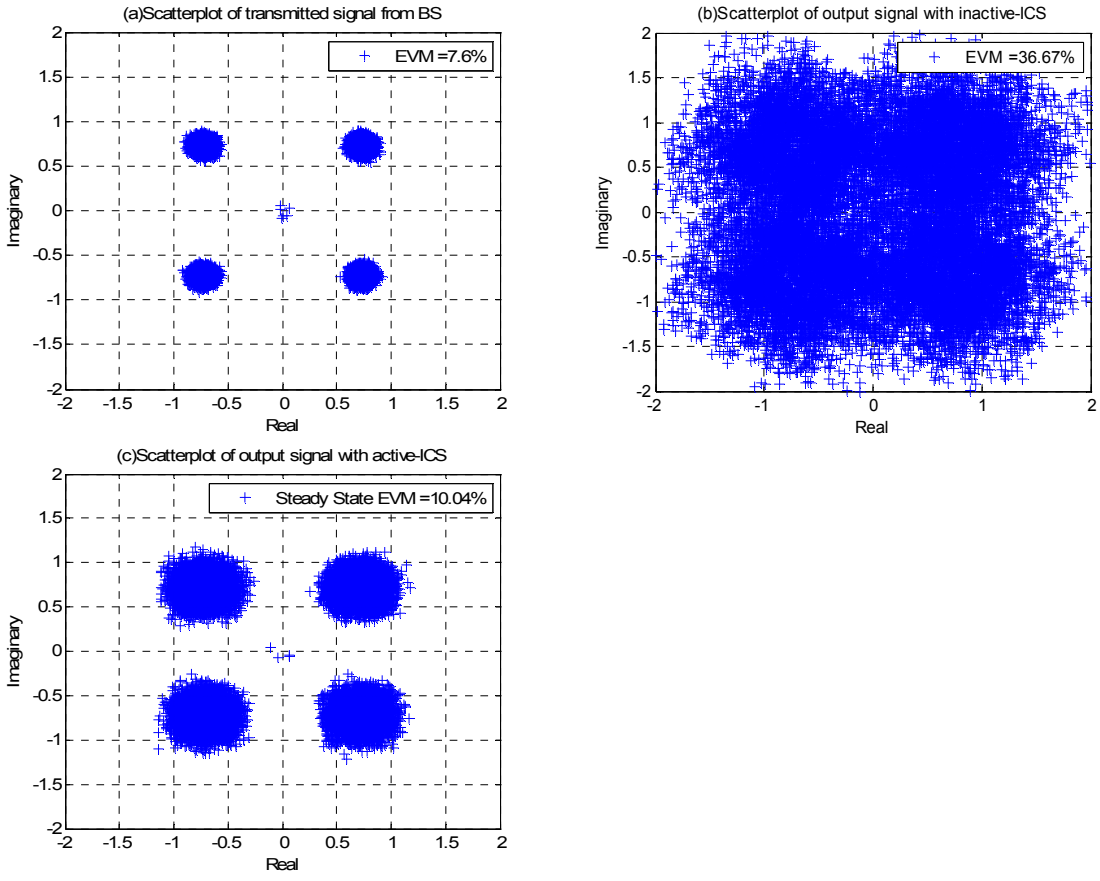

Figure 3.10(a) gives the SER performance of the ICS repeater having one RES, for various values of the SNR, assuming the AWGN and Rayleigh fading channels between the repeater antennas. Figure 3.10(a) shows that the SER is improved for an active ICS. The tracking ability of the ICS repeater is plotted in Figure 3.10(b). Figure 3.10(b) shows that as the radio echo Doppler frequency increases, the MSE degrades. This implies that the ICS fails to track the rapid fluctuations as the fading level increases.

Figure 3.10 Various characteristics plots of ICS

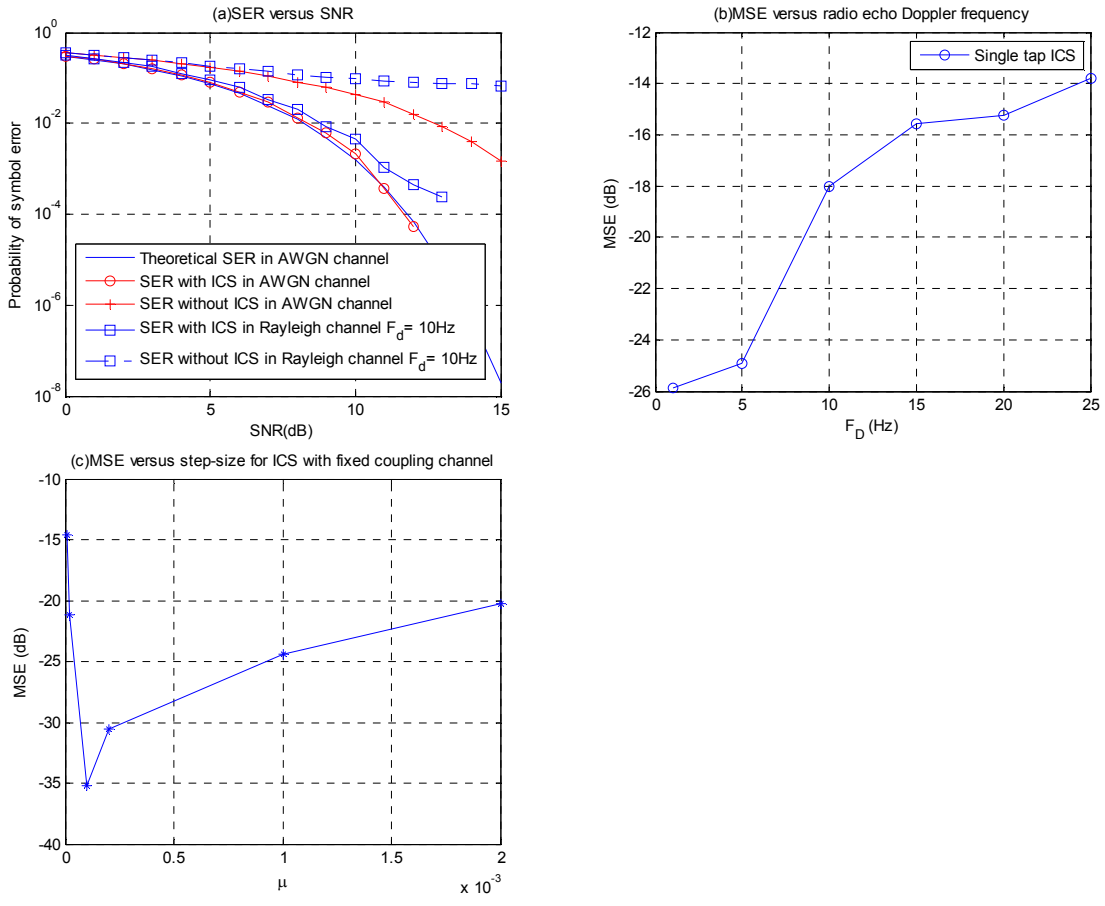

Finally, Figure 3.10(c) presents a plot of the step-size μ versus the MSE, to find the optimum value of the step-size that results in the smallest MSE. The optimum value of the step-size is important since the steady state MSE and the speed of convergence of the adaptive algorithm depend upon it. Figure 3.10(c) shows the optimum step-size factor to be 0.0001.

3.10 Multiple-Tap Radio Echo Suppressor

The ICS algorithm discussed above assumes that the radio echo searcher calculates the perfect delays of the radio echoes. However, the performance of ICS is not addressed in the situation when the delay of the radio echo is estimated incorrectly by integer number of samples. In such a situation, the RES will not suppress the radio echo efficiently. To solve this problem, we introduce a multiple-tap RES structure. Using multiple-taps in the RES gives the advantage of lower MSE, in the situation when the echo searcher gives an incorrect estimate of the radio echo delay, at the expense of slight increase in the ICS repeater complexity. Figure 3.11 shows the block diagram of the multiple-tap RES structure.

MSE of a multiple-tap RES is less than the MSE of a single-tap RES, assuming that there is no sampling error. The MSE of the three-tap RES and five-tap RES is compared with the MSE of a single-tap RES in Figure 3.12, for a radio echo delayed by 100 samples. Figure 3.12 shows that the MSE increases on either side of the correct position of the radio echo. Figure 3.12 also shows that a three-tap RES gives a better performance than a single-tap RES. Likewise, a five-tap

RES works better than a three-tap RES. However, the error floor rises with the additional taps in the RES.

Figure 3.11 Block diagram of multiple-tap RES

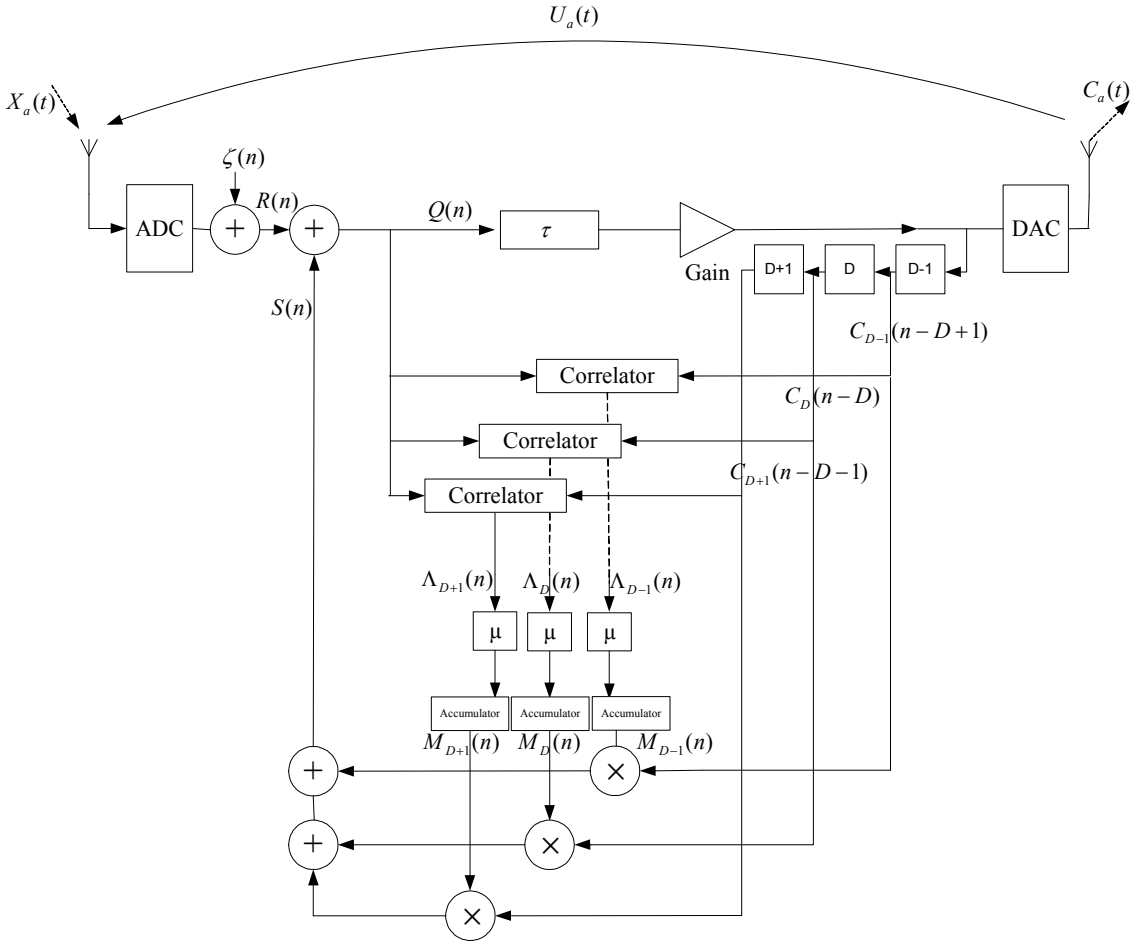

Figure 3.12 MSE of a multiple-tap RES

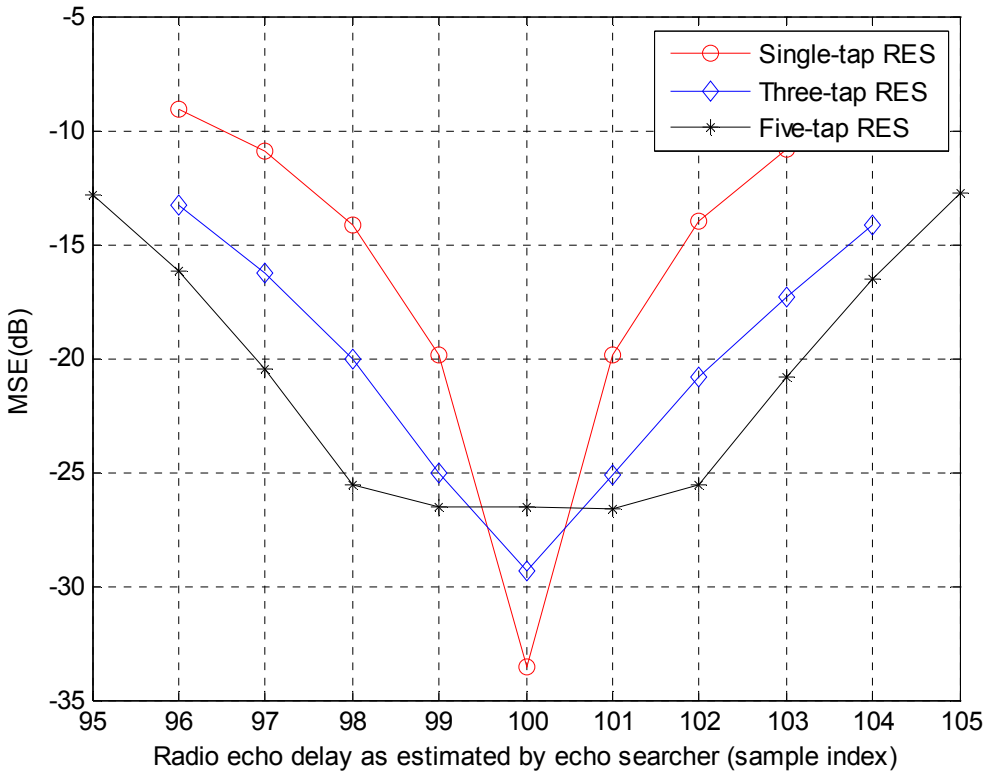

3.11 Summary

This chapter has described the algorithm of the ICS. The main topics covered in this chapter are:

- Working principle of the ICS repeater.
- Criterion of convergence of the ICS algorithm.
- MRES unit and configuration of ICS in real applications.
- Error vector magnitude.
- Different characteristic plots of the ICS algorithm.
- Multiple-tap RES.

CHAPTER 4 RADIO ECHO SEARCHER

4.1 Introduction

This chapter describes the working of the radio echo searcher. The radio echo searcher determines the delays of the dominant echoes in the PDP. It then assigns these delays to the unused radio echo suppressors with the help of the controller. This chapter briefly introduces the radio echo searcher.

4.2 Description

The radio echo searcher measures the arrival time and intensity of the radio echoes. It uses correlation to calculate the PDP. The correlation buffers implemented in this thesis have a resolution of 10.851 ns and can store 1000 samples. The maximum measurable delay is 10.851 μs. For a coupling channel with three multipath components, the received signal $U(n)$ is represented in terms of the transmitted signal $C(n)$ as,

$$U(n) = w_0\, C(n - D_0) + w_1\, C(n - D_1) + w_2\, C(n - D_2)$$

where w_0, w_1 and w_2 are the channel gains, and D_0, D_1 and D_2 are the delays of three echoes respectively. The channel gains are assumed less than unity i.e.

$$w_2 < w_1 < w_0 < 1$$

To estimate the delays of radio echoes, correlation $r_{RC}(\tau)$ is performed between the received signal and the transmitted one i.e.

$$\begin{aligned} r_{RC}(\tau) &= E\{R(n)\ C(n+\tau)\} \\ &= E\{[X(n)+U(n)]\ C(n+\tau)\} \\ &= E\{X(n)\ C(n+\tau)+U(n)C(n+\tau)\} \end{aligned} \quad (4.1)$$

Since the signals $X(n)$ and $C(n+\tau)$ are uncorrelated, we can ignore the first term in Equation 4.1. Equation 4.1 then reduces to,

$$\begin{aligned} r_{RC}(\tau) &= E\{U(n)\ C(n+\tau)\} \\ &= E\{[w_0\ C(n-D_0)+w_1\ C(n-D_1)+w_2\ C(n-D_2)]\ C(n+\tau)\} \\ &= w_0\ r_{CC}(\tau-D_0)+w_1\ r_{CC}(\tau-D_1)+w_2\ r_{CC}(\tau-D_2) \end{aligned} \quad (4.2)$$

Equation 4.2 shows that the correlation of the signals $R(n)$ and $C(n)$ is equal to the sum of the scaled versions of the autocorrelation of the transmitted signal. If $r_{RC}(\tau)$ is plotted against time, it will have peaks at $\tau = D_0$, $\tau = D_1$ and $\tau = D_2$.

The radio echo searcher is capable of detecting an echo with a minimum delay of T_s, which in this thesis equals to 10.851 ns. If delay of the radio echo is smaller than T_s, it will not be detected. Usually, a number of power delay profiles are averaged to get a refined result. Since a limited number of radio echo suppressors are available, not every echo can be assigned to them. Therefore, a threshold value is set on the strength of the detected radio echo. Only that echo which has a magnitude greater than the threshold value is assigned to the available radio echo suppressor.

Figure 4.1 shows the normalized PDP of a coupling channel with three paths. The radio echoes are centered at 100th, 481st and 780th samples

respectively, and correspond to delays of $100 \times T_{symbol}$, $481 \times T_{symbol}$ and $780 \times T_{symbol}$ respectively, where T_{symbol} denotes the symbol time period and equals to $\frac{1}{Data\ rate} = 0.26 \mu s$.

Figure 4.1 Radio echo searcher

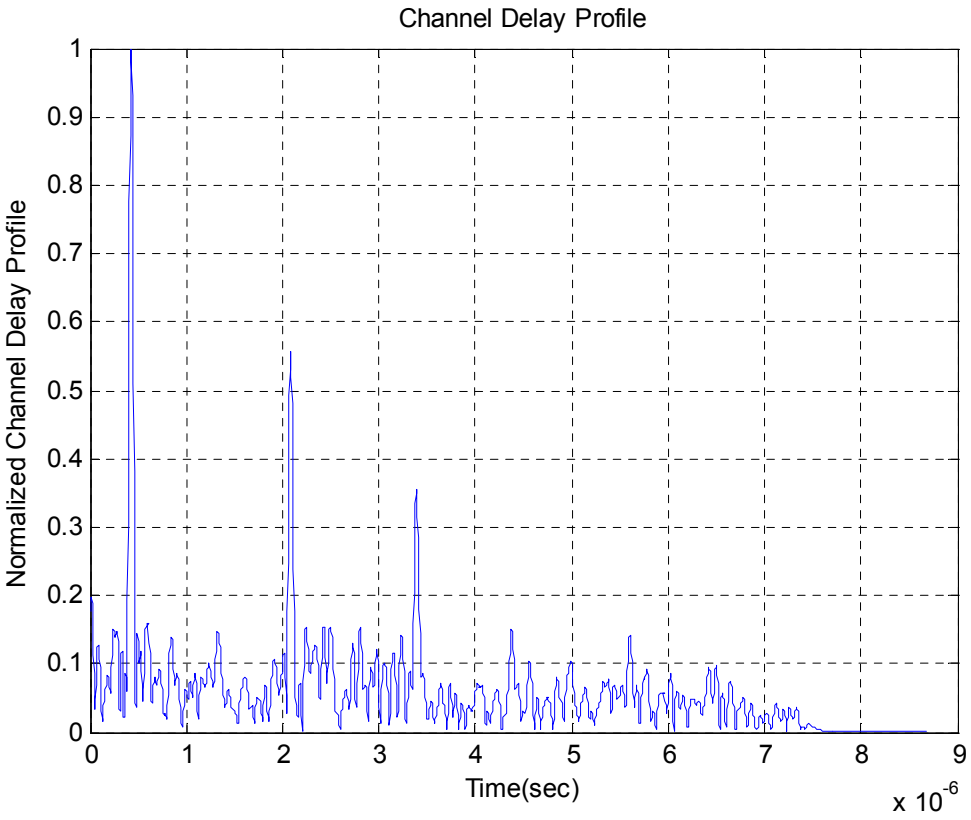

4.3 Summary

This chapter has explained the operation of the radio echo searcher. It is discussed in this chapter that correlation is used to calculate the delays of the radio echoes. The length of the PDP depends upon the size of the correlation

buffers used. Usually, the correlation buffers should be kept long enough to capture significant echoes in the PDP.

CHAPTER 5 FPGA IMPLEMENTATION OF ICS

5.1 Introduction

This chapter discusses the implementation of the ICS algorithm on the field programmable gate array (FPGA). The steps followed to implement the ICS algorithm on the FPGA are described and its suppression capability is measured with the help of the laboratory test equipments.

FPGAs are suitable for real time implementation of the DSP algorithms like ICS because of their high performance, small size, flexibility and competitive price. FPGA consists of programmable logic cells connected together using programmable interconnects. Each cell performs a simple logic function defined by the user's program. These programmable logic cells are used by the FPGA to create a digital circuit. Like microprocessors, FPGAs can be programmed many times. Thus, design revisions can be done easily. Figure 5.1 shows the logic cells of the FPGA arranged in the form of a grid, with programmable interconnects between them. FPGA usually comes as a part of some development board. The development board provides interface to the real world applications. The board contains ADCs, DACs, onboard memory and external USB interface. The FPGA used in this thesis is the Xilinx Virtex-4 FPGA.

Figure 5.1 Logic cells of FPGA

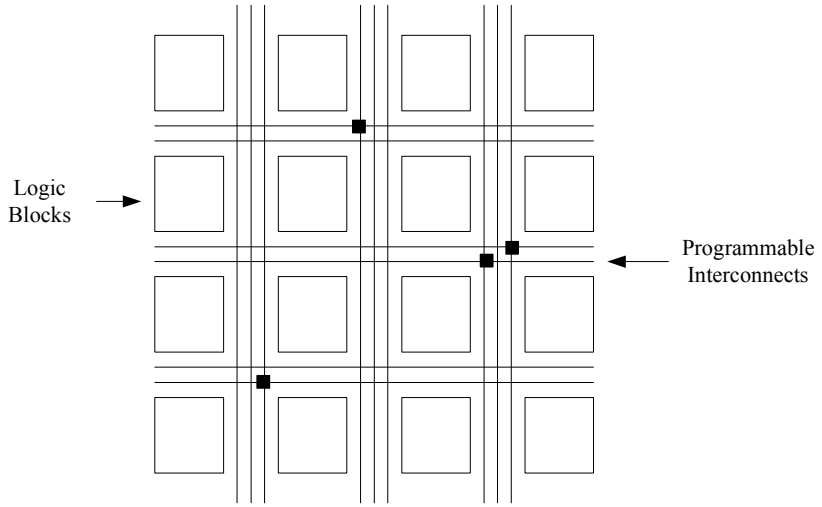

5.2 XtremeDSP Development Kit-IV

The XtremeDSP Development Kit-IV by Nallatech is a platform for the Virtex-4 FPGA. It is an industrial choice for high performance DSP applications [16]. Figure 5.2 shows the internal view of the XtremeDSP Development Kit-IV. The key components of this development board are the following [16]:

- Virtex-4 main user FPGA (Virtex-4 XC4VSX35-10FF668)
- Virtex-II clock FPGA (Virtex-II XC2V80-4CS144)
- Spartan-II interface FPGA
- Two 14-bit independent ADC channels (AD6645 ADC)
- Two 14-bit independent DAC channels (AD9772 DAC)
- Support for external clock, on board oscillator and programmable clock

The system designed by the user is mapped into the Virtex-4 FPGA. The Virtex-II FPGA is used as a clock configuration device in the design [16]. The ADCs and DACs are clocked using the onboard oscillator. The frequency of the onboard oscillator controls the maximum sampling rate of the ADCs and DACs. The ADCs

can be clocked up to 105 MHz whereas the DACs can go up to 160 MHz [16].

Figure 5.2 Internal view of XtremeDSP Development Kit-IV

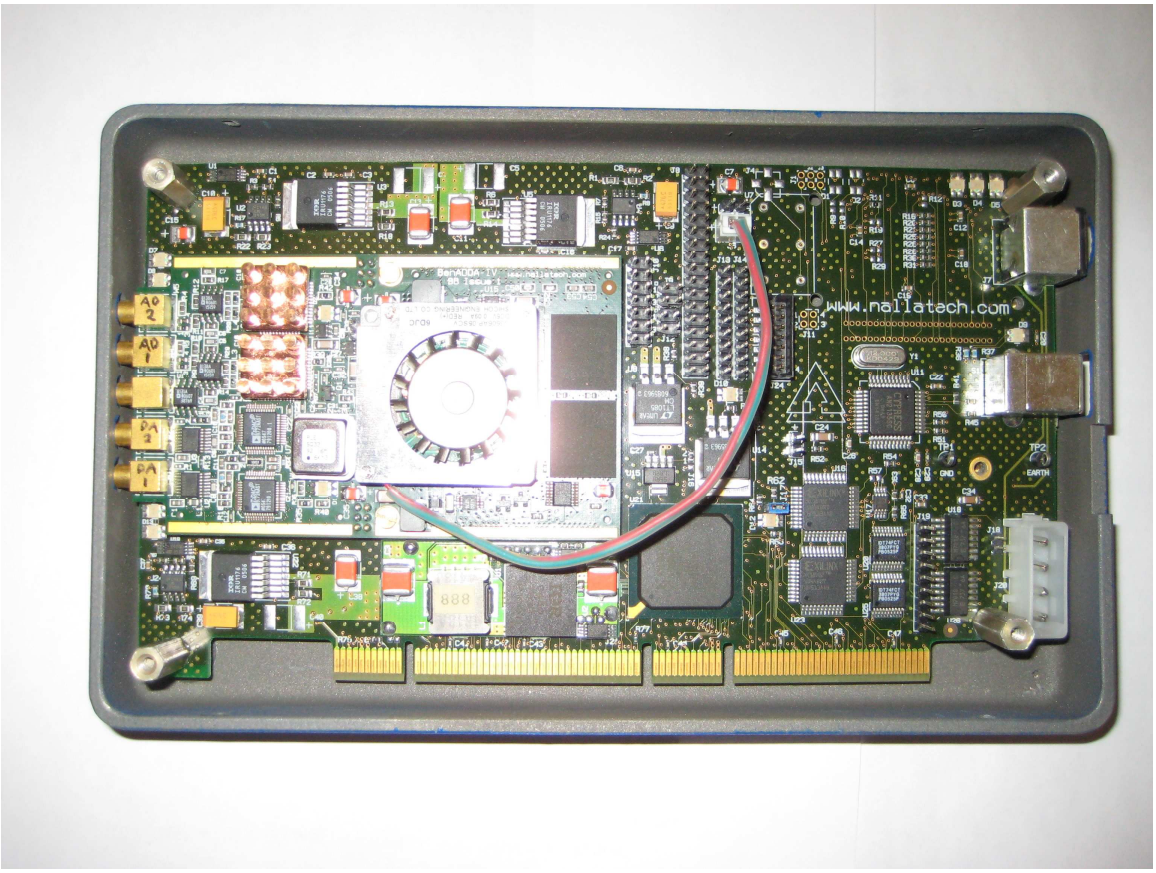

5.3 Design Flow

Figure 5.3 shows the design flow diagram used to implement the ICS algorithm on the FPGA. The description of each block is mentioned below,

- **MATLAB**

  MATLAB is used to simulate the ICS algorithm and study its various features. MATLAB is a high-level scientific and engineering programming environment that has an extensive library of built-in functions for data manipulations.

- **Simulink**

  Simulink is used to graphically layout the ICS algorithm using a customizable set of block libraries. Simulink makes it easy to understand the functional behaviour of the ICS repeater.

- **Xilinx System Generator**

  Xilinx System Generator is a modeling tool used to facilitate the FPGA hardware design. The Xilinx System Generator comes as a library in the Simulink. Xilinx System Generator blocks are bit-accurate [16]. This implies that the Xilinx System Generator blocks produce values in the Simulink that match the corresponding values produced in the hardware. The Xilinx System Generator automatically generates an optimized VHDL code. This VHDL code is synthesized using the Xilinx ISE to produce a binary file that can be programmed into the FPGA.

- **Xilinx ISE**

  The Xilinx integrated software environment (ISE) synthesizes the digital design into a binary file suitable for the FPGA. The digital design consists of a number of VHDL files generated by the Xilinx System Generator including the digital clock manager (DCM) and the user constraints file (UCF). The UCF file is an ASCII file specifying the constraints on the digital design [17]. In the Xilinx ISE, these constraints are used to map the digital design into the FPGA.

- **FPGA Test Bench**

  The test bench includes a digital down convertor (DDC), a digital up convertor (DUC) and an XtremeDSP Development Kit-IV. Other measurement equipments like an oscilloscope, a signal generator and a spectrum analyzer are also used. Section 5.4 gives an elaborate discussion on the lab test bench.

Figure 5.3 Design flow of algorithm

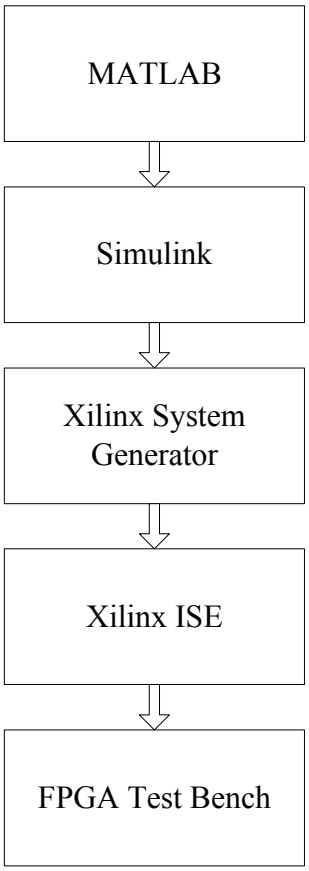

5.4 Laboratory Test Bench

A block diagram of the laboratory test bench is given in Figure 5.4. The development board is XtremeDSP Development Kit-IV having a Virtex-4 FPGA. The Rohde and Schwarz SMIQ03B signal generator is used to generate RF WCDMA signal. This RF signal is passed through the ADC1 of the FPGA. The clock frequency of the FPGA is set to 92.16 MHz. In the FPGA, the DDC converts the RF signal into inphase and quadrature baseband signals. The inphase and quadrature signals act as inputs to the ICS module. After processing by the cancellation algorithm, the inphase and quadrature signals are modulated back to RF using the DUC. The spectrum of the RF signal is displayed using the Rohde and Schwarz FSQ 8 signal analyzer.

In this entire experiment, the variance of the RF signal is fixed at 0.1. A fixed tap coupling channel, which is 8 dB less than the power of the incoming signal, is realized within the FPGA. The XtremeDSP Development Kit is connected to the host PC using a parallel-IV cable and programmed using the ChipScope programming and debugging tool. Figure 5.5 contains a photograph of the laboratory test bench. The parameters used in the test bench are listed in Table 5.1.

Figure 5.4 Laboratory test bench

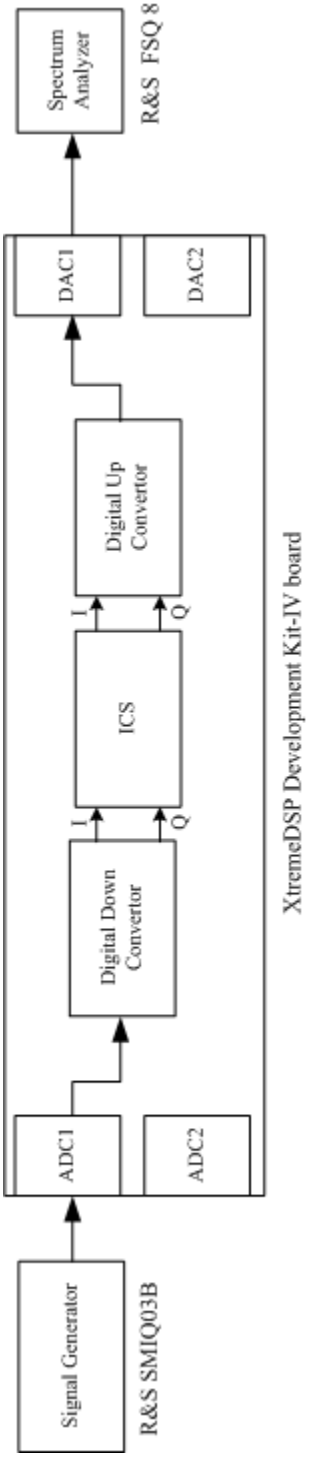

Figure 5.5 Photograph of laboratory test bench

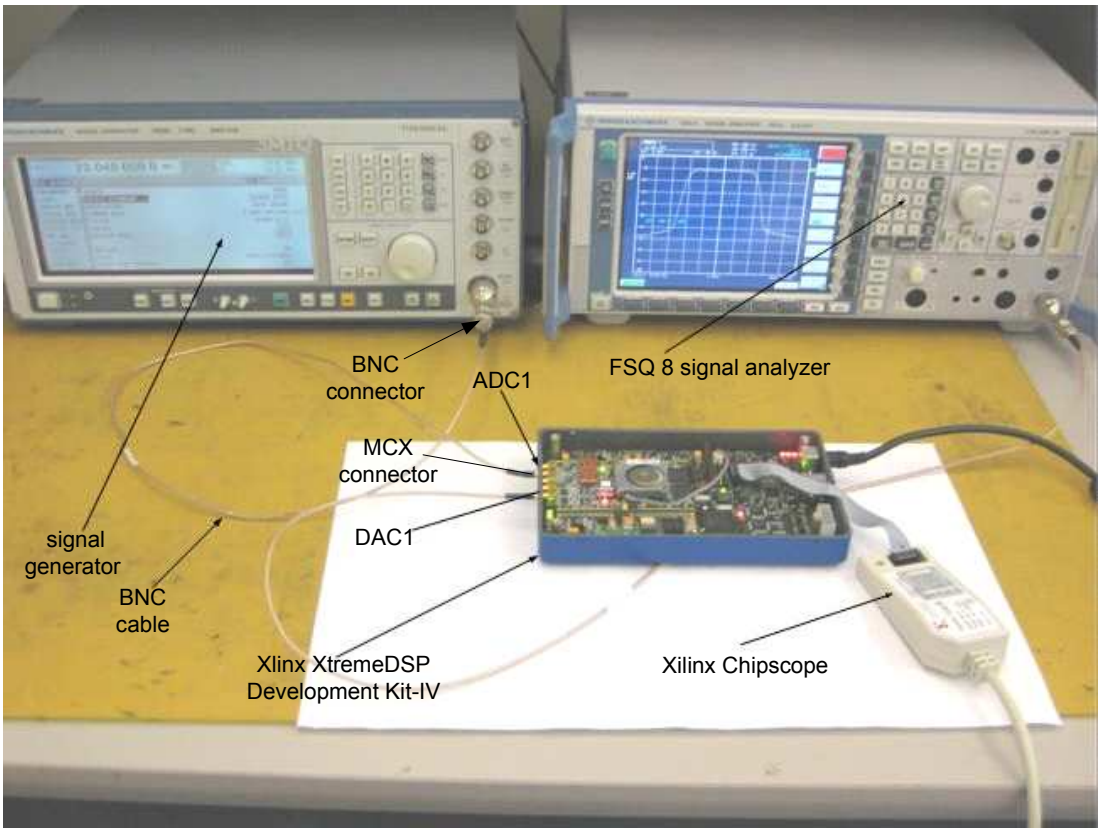

Table 5.1 Parameters used in test bench

Quantity	Value	Remarks
FPGA clock frequency	92.16 MHz	Onboard oscillator
ADC sampling frequency	92.16 MHz	
DAC sampling frequency	92.16 MHz	
WCDMA signal data rate	3.84 MSPS	Modulated WCDMA carrier
Sampling rate of WCDMA	38.4 MHz	
Bandwidth of WCDMA	5 MHz	
Number of carriers in WCDMA	1	Single carrier WCDMA
Number of RES	1	
Number of radio echoes	1	
RF signal carrier frequency	23.04 MHz	
SMIQ signal level	6.2 dBm	
FSQ reference level	0 dBm	

5.5 Measurement Results

Figure 5.6 shows the tracking performance of the ICS in the FPGA for a fixed tap coupling channel. Figure 5.7 shows the learning curve of the ICS. Figure 5.8 gives the spectrum of the input signal whereas Figure 5.9 represents the demodulated signal spectrum. Figure 5.10 shows the frequency response of the coupling channel. The spectra of the output signal and error signal are given in Figure 5.11 and Figure 5.12 respectively. Table 5.2 compares the FPGA and MATLAB simulation results. Table 5.2 shows that the interference cancellation using the FPGA is 13 dBc; that agrees with the MATLAB results. Due to the presence of quantization noise and limited floating point precision, the FPGA results can differ slightly from the MATLAB ones. The cancellation ability of the ICS repeater is determined by taking the absolute value of the difference between the average value of the interference signal and the average value of the error signal. The unit of the interference cancellation is in decibels relative to interference (dBc).

Figure 5.6 Tracking performance of single-tap ICS in FPGA

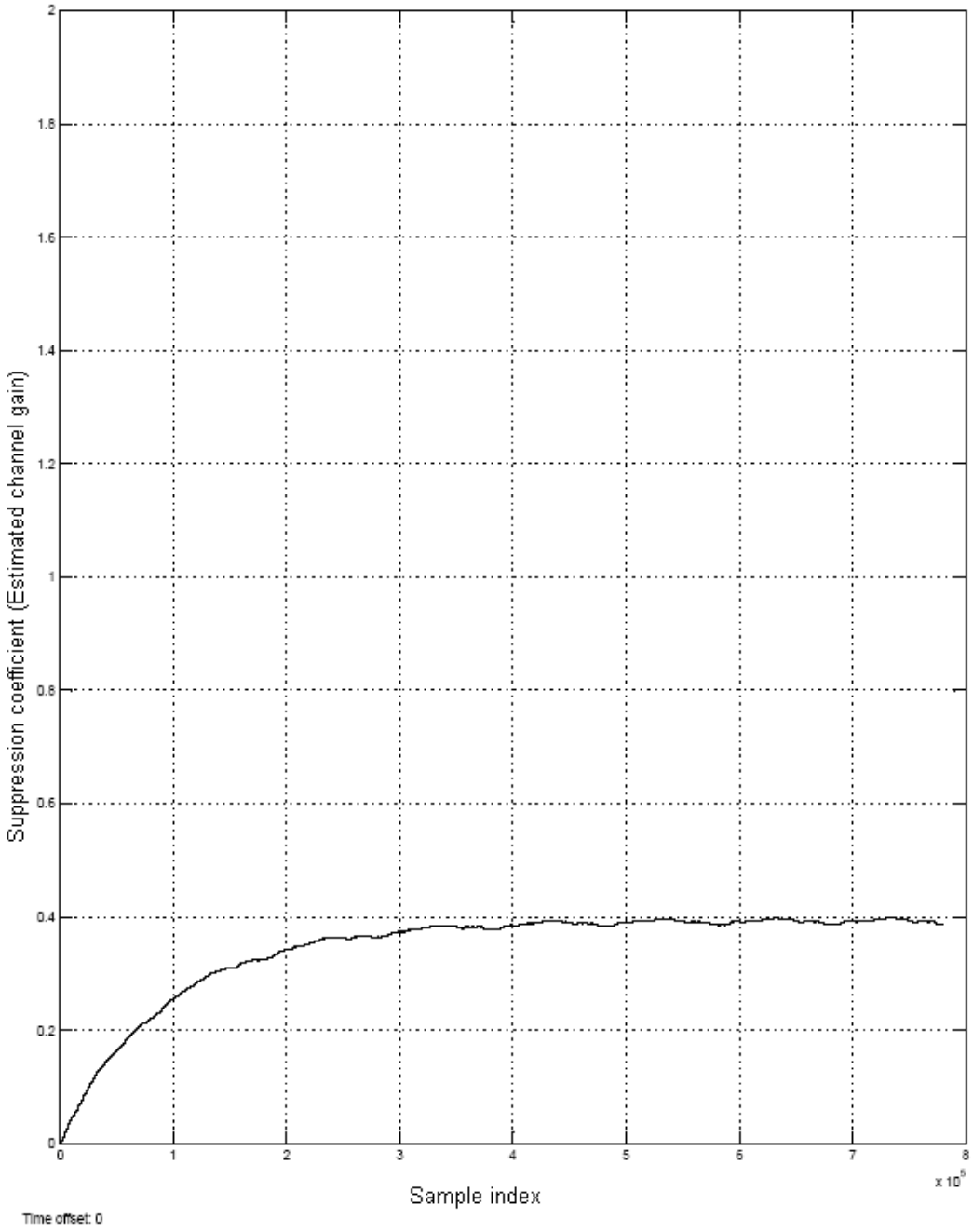

Figure 5.7 Learning curve for single-tap ICS when used to track a fixed tap channel

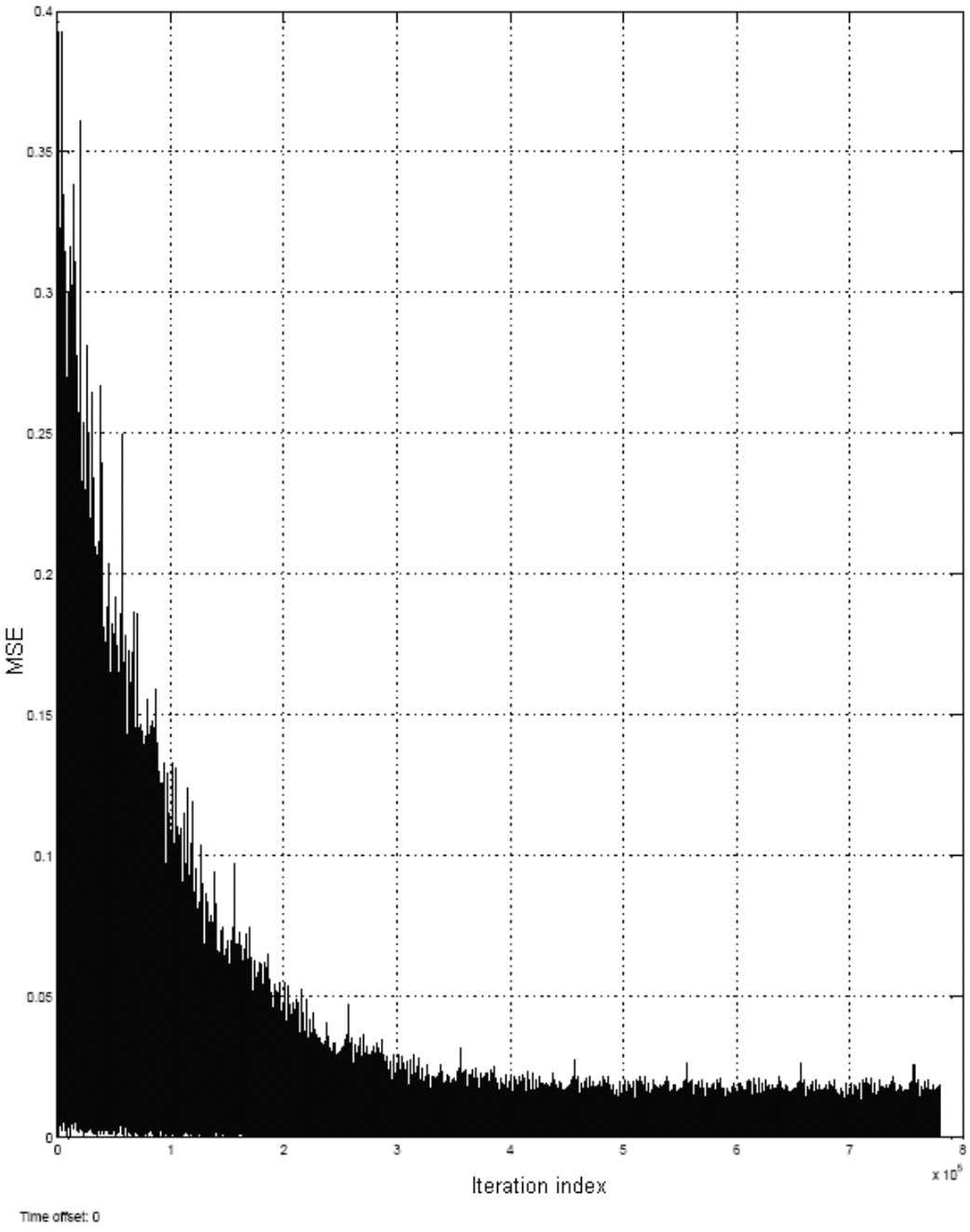

Figure 5.8 Spectrum of input signal

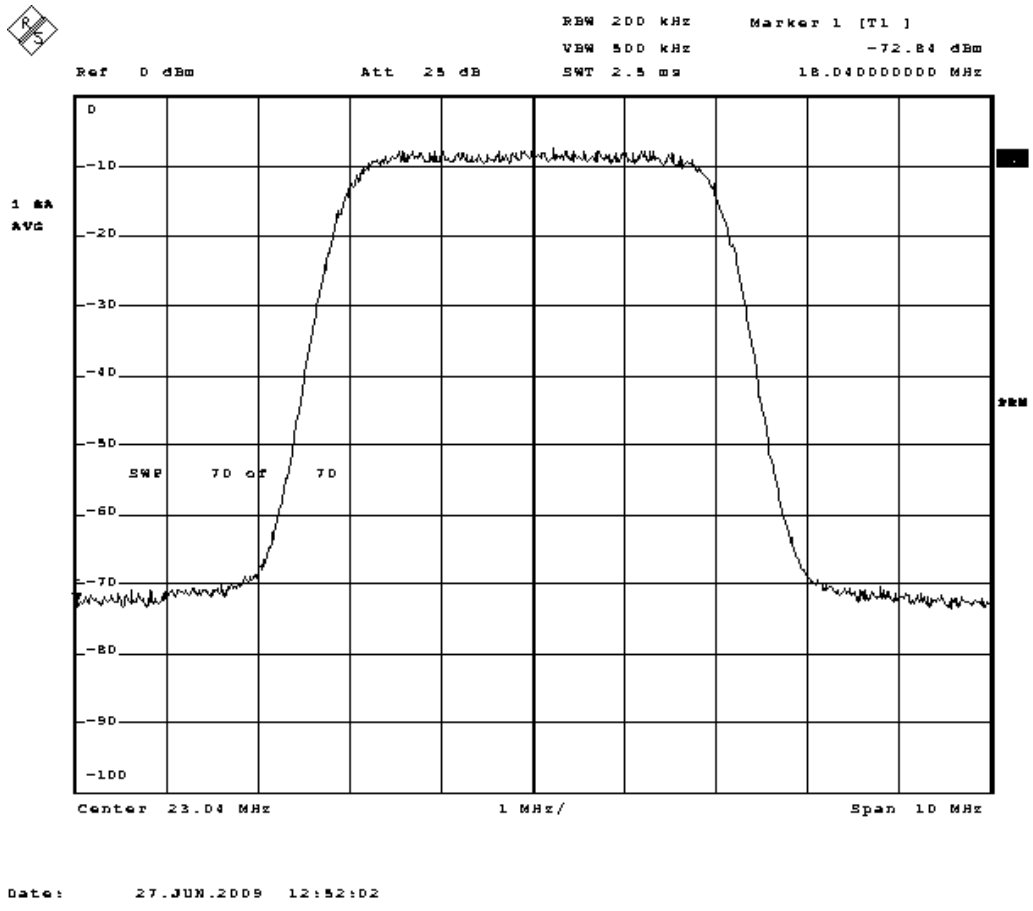

Figure 5.9 Spectrum of baseband signal

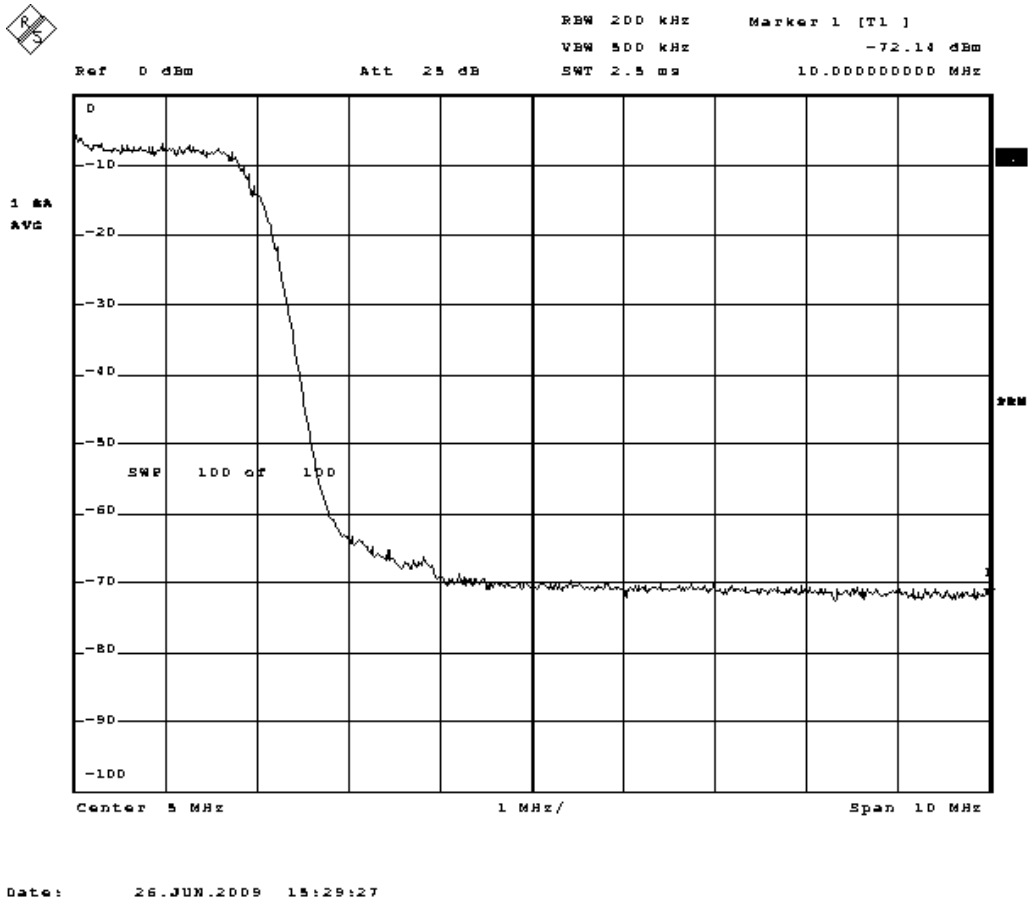

Figure 5.10 Spectrum of coupling signal

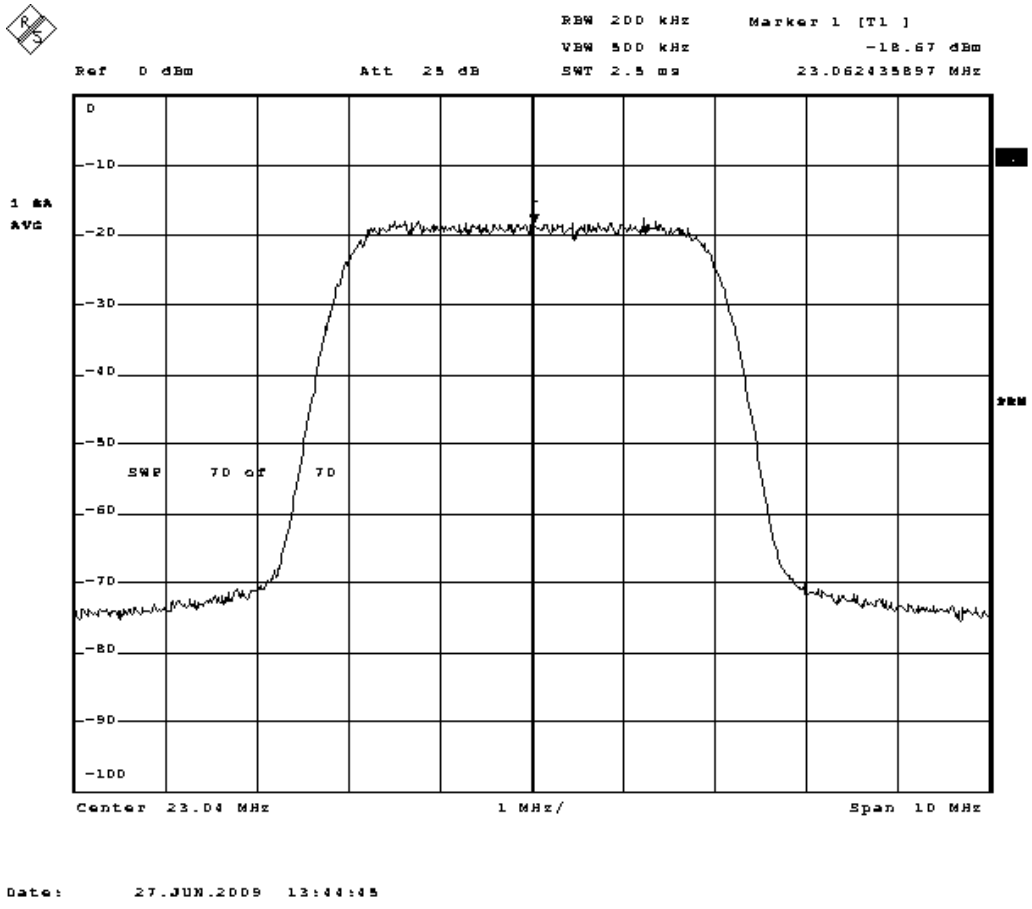

Figure 5.11 Spectrum of output signal

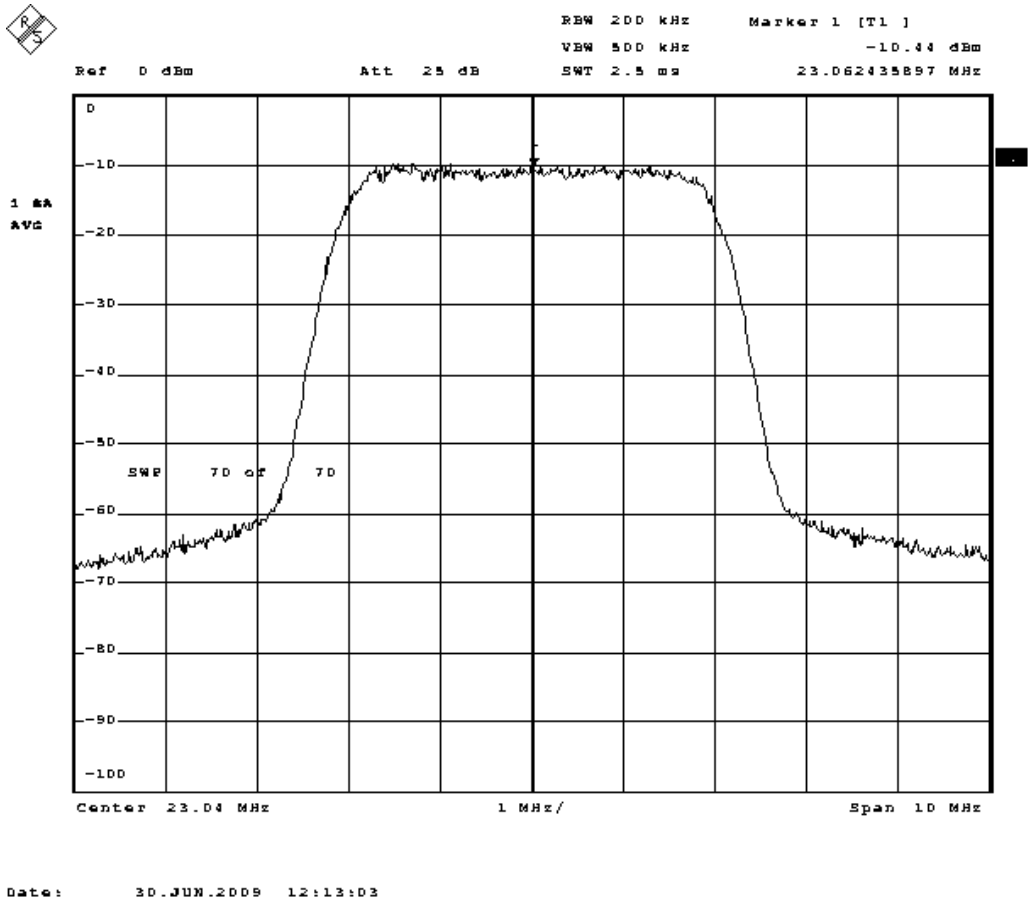

Figure 5.12 Spectrum of error signal

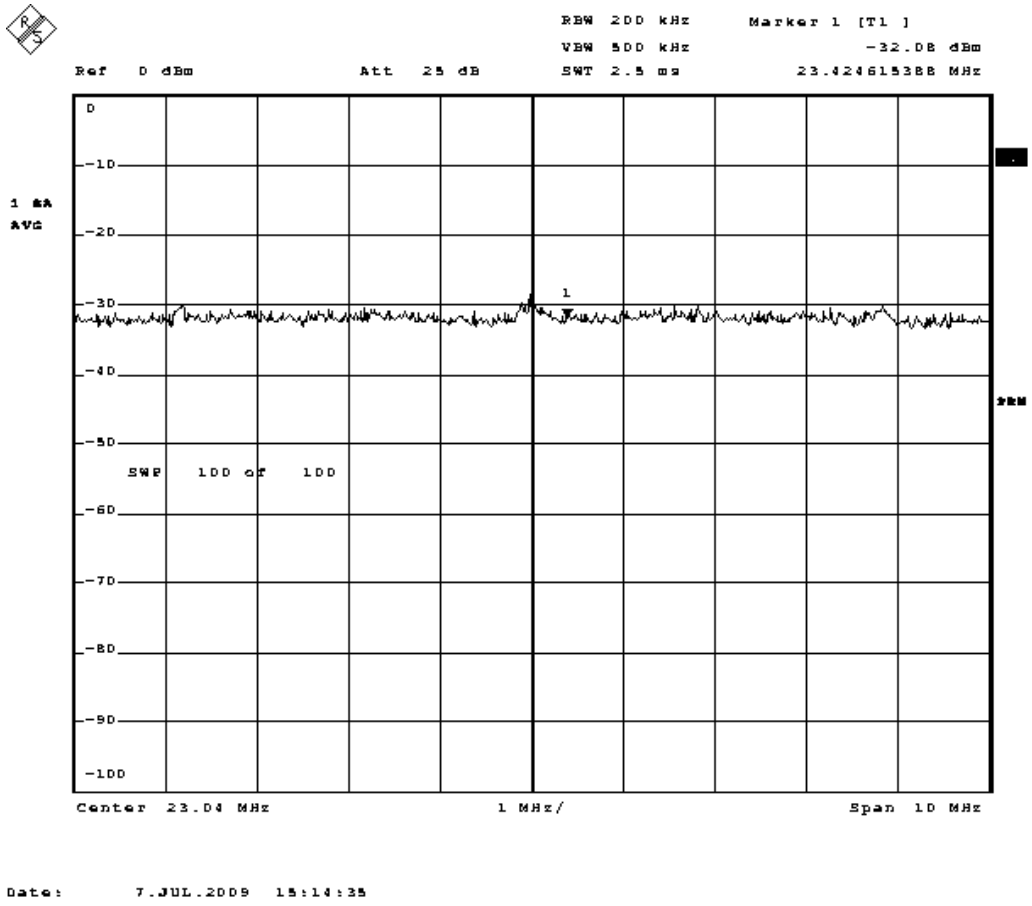

Table 5.2 Comparison between MATLAB and FPGA results

Signal	MATLAB	FPGA
Transmitted signal from BS	29.14 dBm	-12 dBm
Interference signal	13.95 dBm	-20 dBm
Error signal	0.56 dBm	-33 dBm
Cancellation relative to interference	13.39 dBc	13 dBc

5.6 FPGA Resource Utilization

The Xilinx ISE generates a number of reports during the synthesis process. Device utilization summary listed in Table 5.3 gives the resource utilization of the ICS algorithm on the FPGA.

Table 5.3 Resource utilization by ICS algorithm

	Logic utilization	Available	Percentage
Number of slice Flip Flops	4190	30720	13%
Number of four input LUTs	9896	30720	32%
Number of DSP48 blocks	38	192	19%

Table 5.3 shows that 13% flip-flops, 32% look up tables (LUTs) and 19% DSP48 blocks are utilized in the FPGA. An important parameter in the resource utilization summary is the consumption of the DSP48 blocks. The DSP48 blocks are highly efficient blocks created specifically for the DSP applications and use the Xilinx Virtex-4 devices [16]. Each DSP48 slice contains a dedicated signed multiplier, an adder logic, and a 48-bit accumulator. The multiplier and accumulator can be used independently. DSP48 blocks are designed to implement high-speed DSP applications.

5.7 Summary

This chapter describes the implementation of the ICS on the FPGA. The main points discussed in this chapter are:

- The combination of MATLAB, Simulink and Xilinx ISE provides a powerful method for developing and testing the DSP algorithms on the FPGA.

- The suppression performance of the ICS repeater having a single-tap RES with an input signal of variance 0.1 is 13 dBc that coincides with the simulated result.

CHAPTER 6 CONCLUSION

This thesis has described a solution for the problem of coupling in the 3G wireless repeaters. The ICS presented here does not require any training sequence or pilot symbols. It has far less complexity than the other interference cancellation approaches. The MATLAB simulations show that the proposed ICS works fairly well in the flat and frequency selective fading channels. In the ICS, the steepest descent algorithm is used to estimate the gain of the channel. This thesis has also introduced a modified RES, which has multiple-taps in it. The multiple-taps RES is better than the single-tap RES as shown in the simulation.

The ICS algorithm is also realized on the Virtex-4 FPGA. The MATLAB simulation and FPGA results are compared with a high degree of agreement. The Xilinx System Generator and ISE are found as useful tools for developing the ICS in the FPGA.

This thesis can be improved in the following areas:

- The steepest descent algorithm is suboptimal in nature and can be replaced by optimal channel tracking algorithms e.g., Kalman filter.
- The complexity of the ICS can be addressed. Simple techniques can be developed for fast processing.
- More sophisticated and accurate algorithms for the radio echo searcher can be introduced.
- ICS for multi-carrier WCDMA can be developed.

- SISO implementation of the ICS can be extended to MIMO implementation.

APPENDICES

APPENDIX 1

$$MSE_{sytem} = E\left\{\left|\varepsilon_{system}(n)\right|^2\right\}$$
$$= E\left\{\left|U(n) + S(n)\right|^2\right\}$$

where,

$$U(n) = w_l \times C(n-D)$$
$$S(n) = M_l \times C(n-D)$$

$$MSE_{sytem} = E\left\{\left|U(n) + S(n)\right|^2\right\}$$
$$= E\left\{\left|C(n-D) \times (w_l + M_l)\right|^2\right\}$$
$$= E\left\{\left|C(n-D)\right|^2\right\} \times E\left\{\left|(w_l + M_l)\right|^2\right\}$$

$$E\left\{\left|C(n-D)\right|^2\right\} = E\left\{\left|C(n)\right|^2\right\} = \sigma^2$$

$$MSE_{sytem} = \sigma^2 \times E\left\{\left|(w_l + M_l)\right|^2\right\}$$

$$MSE = E\left\{\left|(w_l + M_l)\right|^2\right\}$$

$$MSE = \frac{MSE_{sytem}}{\sigma^2}$$

$$MSE_{dB} = 10\log_{10}\left(\frac{MSE_{system}}{\sigma^2}\right)$$
$$= 10\log_{10}(MSE_{system}) - 10\log_{10}\left(\sigma^2\right)$$
$$= MSE_{system\_dB} - 10\log_{10}\left(\sigma^2\right)$$

APPENDIX 2

$$\begin{aligned}\varepsilon_{sytem}(n) &= U(n) + S(n) \\ &= C(n-D)\times(w_l + M_l)\end{aligned}$$

$$w = |w_l| e^{j\phi_{w_l}}$$

$$M_l = |M_l| e^{j\phi_{M_l}}$$

$$\begin{aligned}\varepsilon_{sytem}(n) &= C(n-D)\times(w_l + M_l) \\ &= C(n-D)\times\left(|w_l| e^{j\phi_{w_l}} + |M_l| e^{j\phi_{M_l}}\right)\end{aligned}$$

$$|M_l| \approx |w_l|$$

$$\phi_{M_l} \approx |\phi_{w_l}| \pm \pi$$

$$\begin{aligned}\varepsilon_{sytem}(n) &= C(n-D)\times\left(|w_l| e^{j\phi_{w_l}} + |M_l| e^{j(\phi_{w_l}\pm\pi)}\right) \\ &= C(n-D)\times\left(|w_l| e^{j\phi_{w_l}} + |M_l| e^{j\phi_{w_l}} e^{\pm j\pi}\right) \\ &= C(n-D)\times e^{j\phi_{w_l}}\left(|w_l| - |M_l|\right)\end{aligned}$$

APPENDIX 3

System Generator block diagram of interference cancellation system

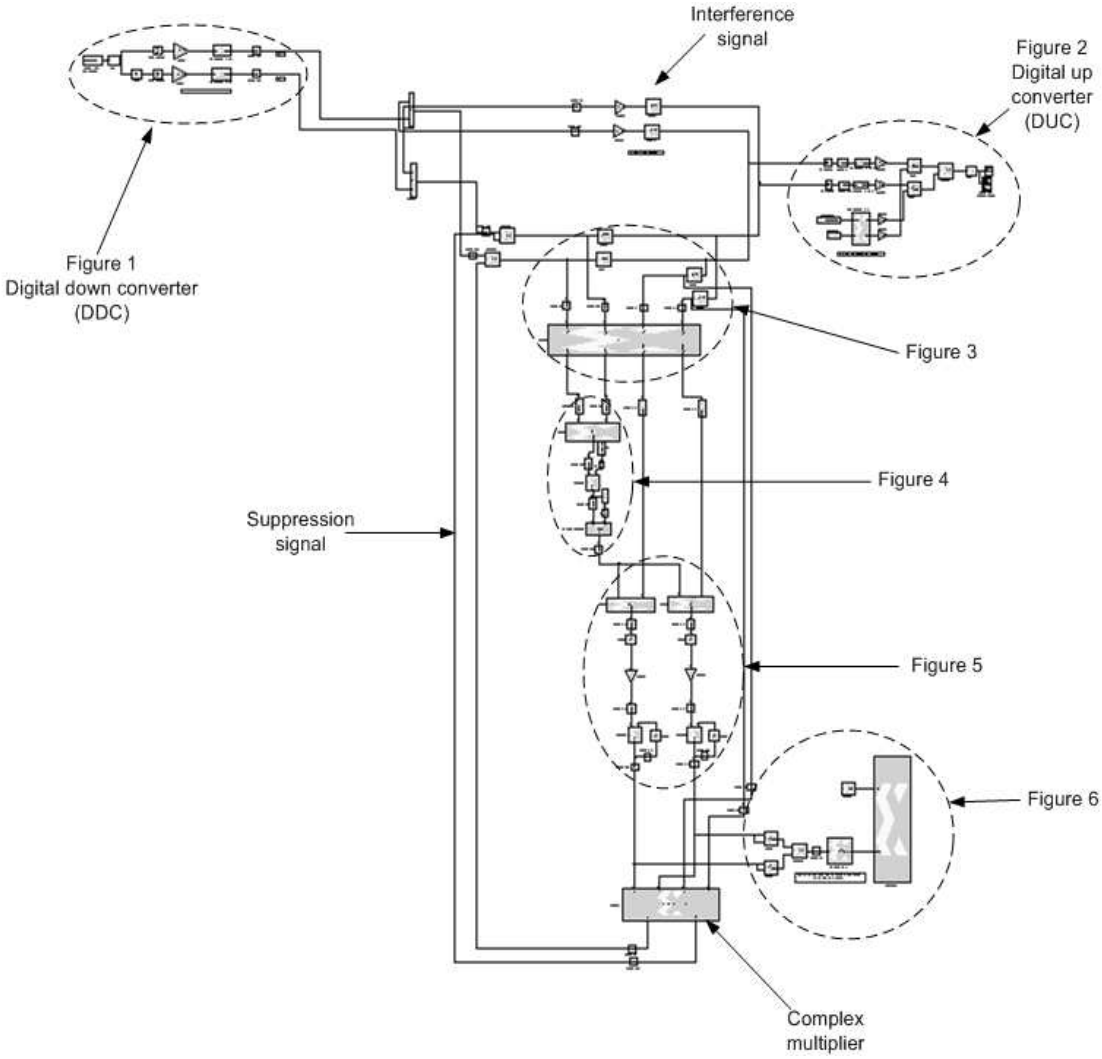

Figure 1

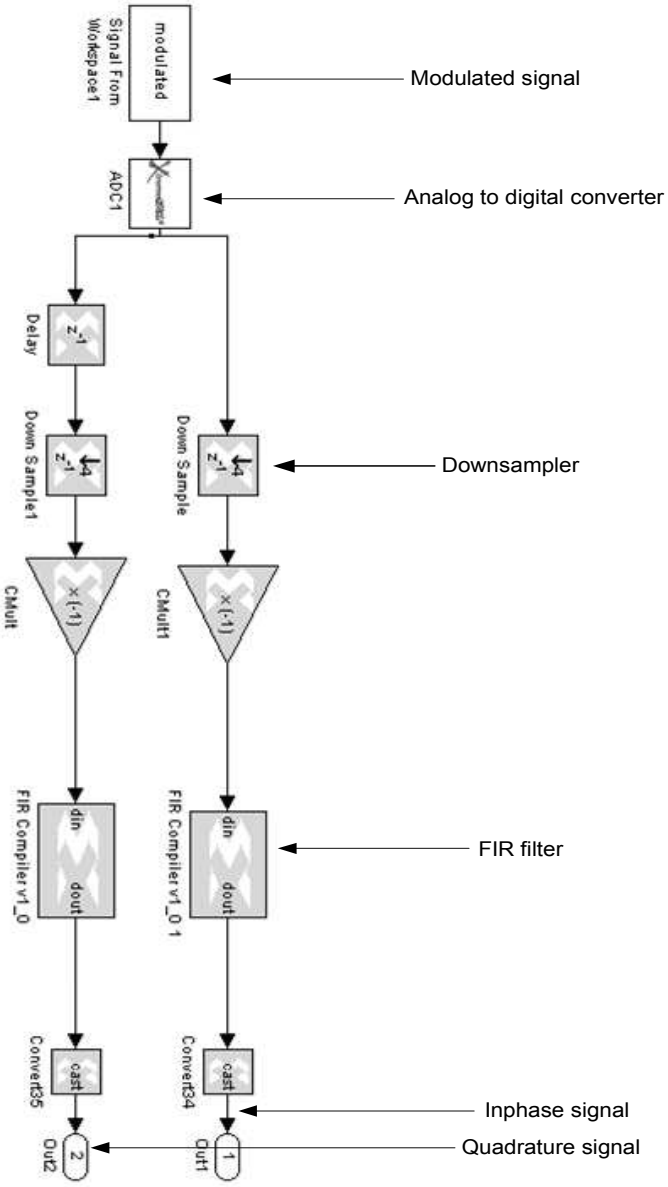
Signal From Workspace1
modulated
Modulated signal
ADC1
Analog to digital converter
Delay
Down Sample1
Down Sample
Downsampler
CMult
CMult1
FIR Compiler v1_0
FIR Compiler v1_0 1
din
dout
FIR filter
Convert35
Convert34
cast
Inphase signal
Out2
Out1
Quadrature signal

Figure 2

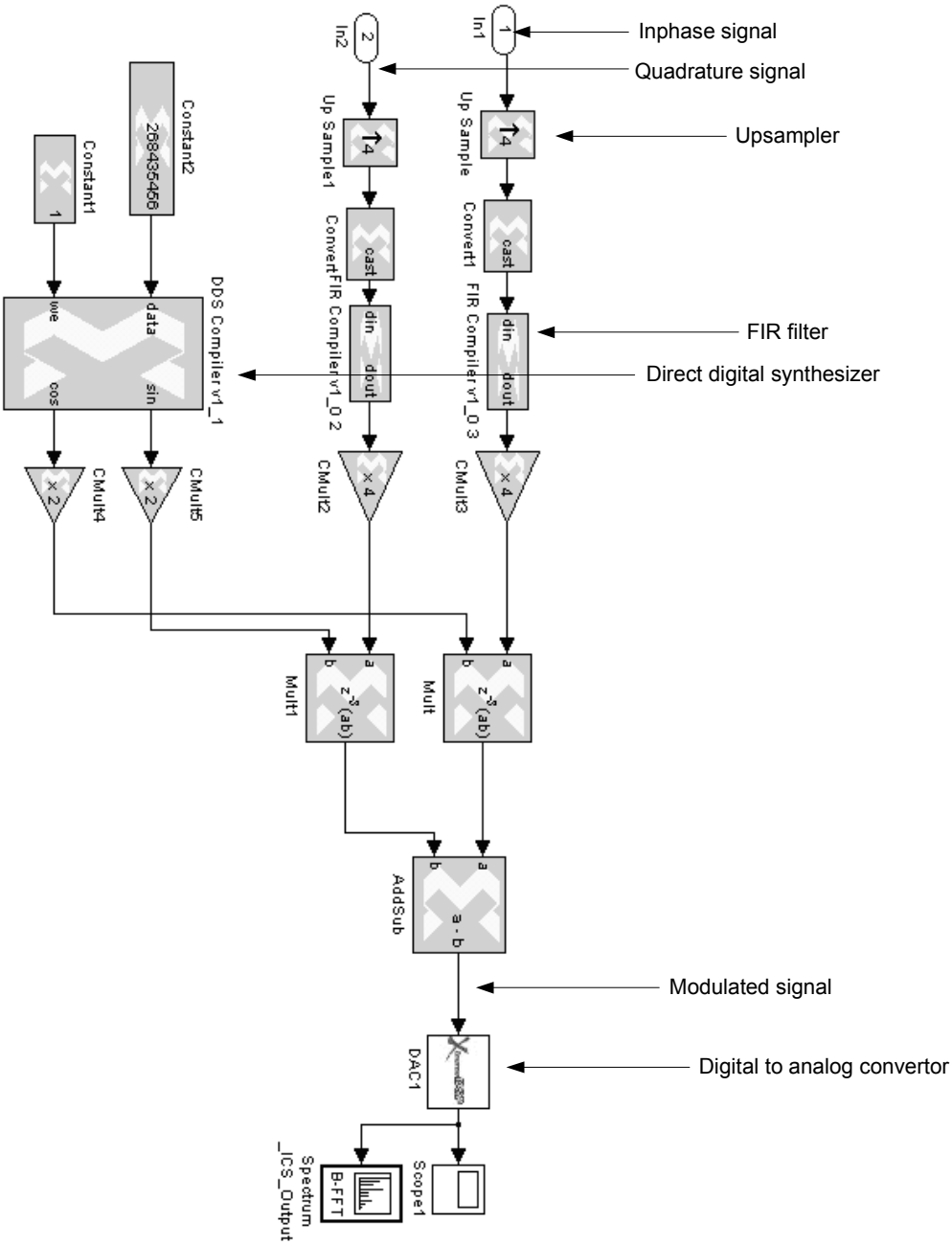
In1
In2
Inphase signal
Quadrature signal
Up Sample
Up Sample1
Upsampler
Convert1
ConvertFIR Compiler v1_0 2
FIR Compiler v1_0 3
FIR filter
Constant1
Constant2
DDS Compiler v1_1
Direct digital synthesizer
CMult4
CMult5
CMult2
CMult3
Mult1
Mult
AddSub
Modulated signal
DAC1
Digital to analog convertor
B-FFT
Spectrum_ICS_Output
Scope1

Figure 3

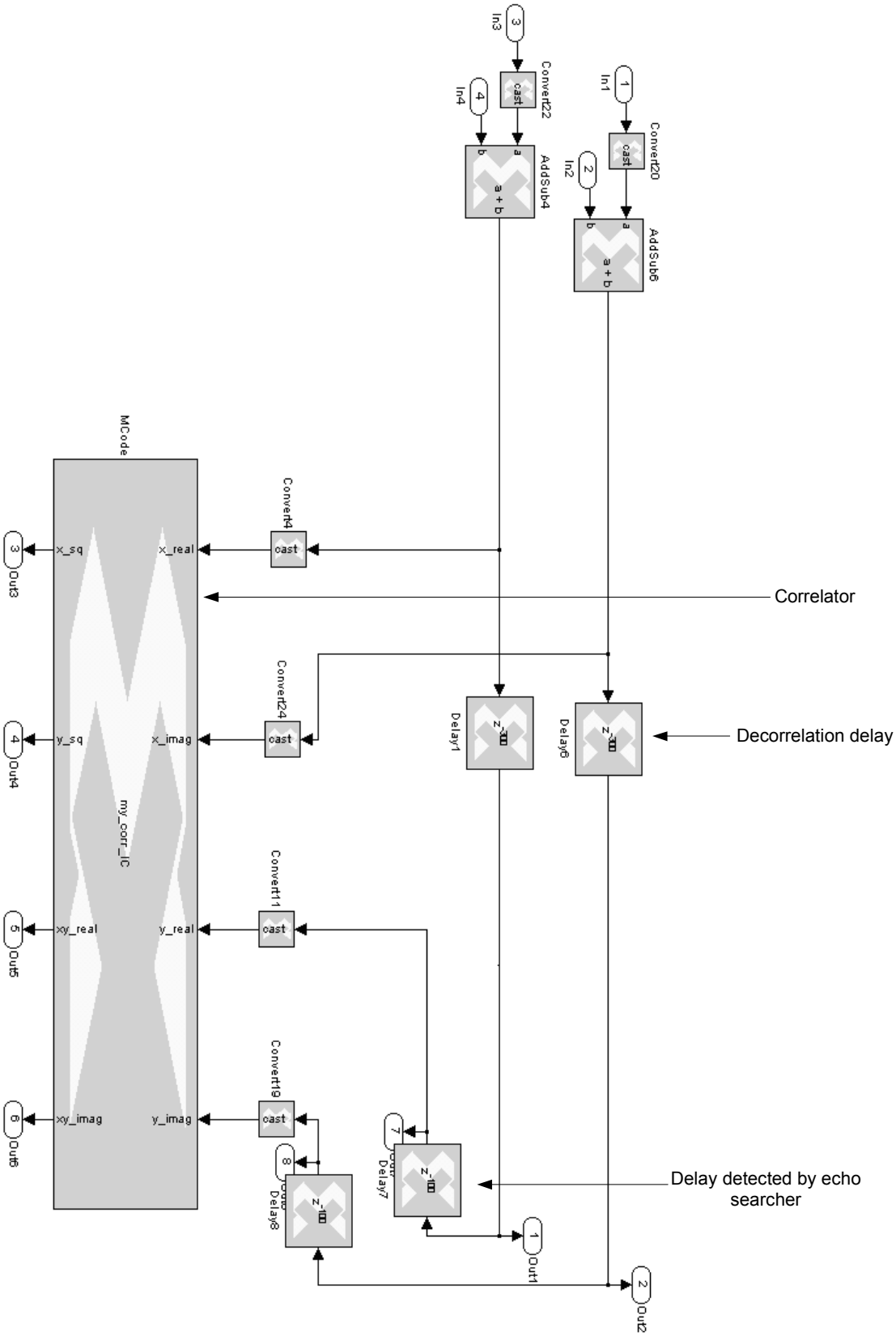
In3
In4
In1
In2
Convert22
Convert20
AddSub4
AddSub6
MCode
Convert4
Convert24
Convert11
Convert19
x_sq
x_real
y_sq
x_imag
xy_real
y_real
xy_imag
y_imag
my_corr_IC
Out3
Out4
Out5
Out6
Out1
Out2
Delay1
Delay6
Delay7
Delay8
Correlator
Decorrelation delay
Delay detected by echo searcher

Figure 4

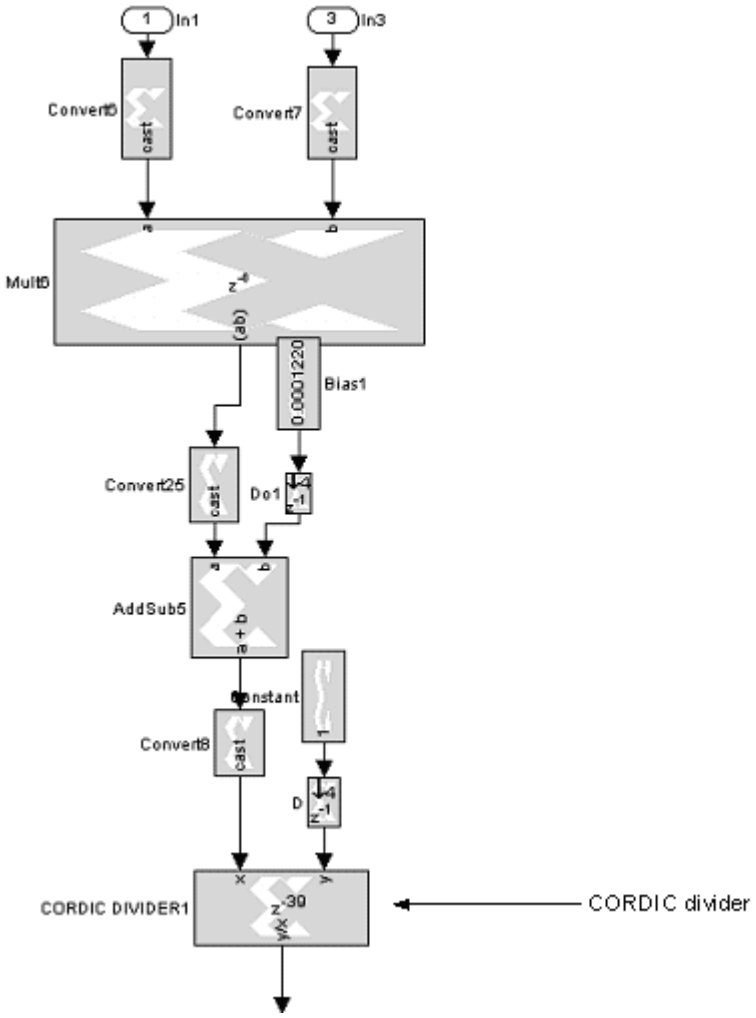
1
In1
3
In3
Convert5
cast
Convert7
cast
a
b
Mult5
z^-4
(ab)
0.0001220
Bias1
Convert25
cast
Do1
a
b
AddSub5
a + b
Constant
1
Convert8
cast
D
x
y
CORDIC DIVIDER1
z^-30
y/x
CORDIC divider

Figure 5

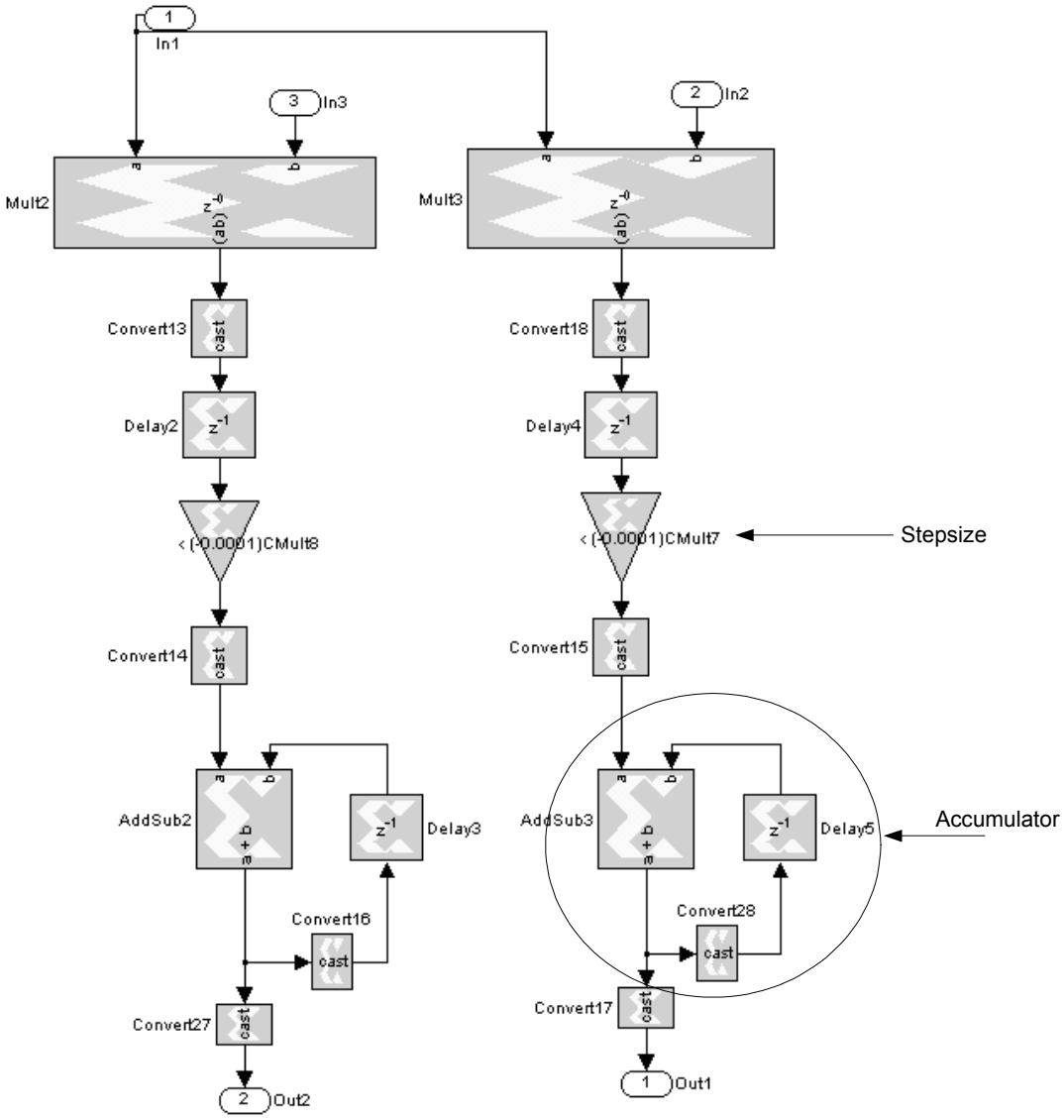
1
In1
3
In3
2
In2
Mult2
Mult3
Convert13
Convert18
Delay2
Delay4
<(-0.0001)CMult8
<(-0.0001)CMult7
Stepsize
Convert14
Convert15
AddSub2
AddSub3
Delay3
Delay5
Accumulator
Convert16
Convert28
Convert27
Convert17
2
Out2
1
Out1

Figure 6

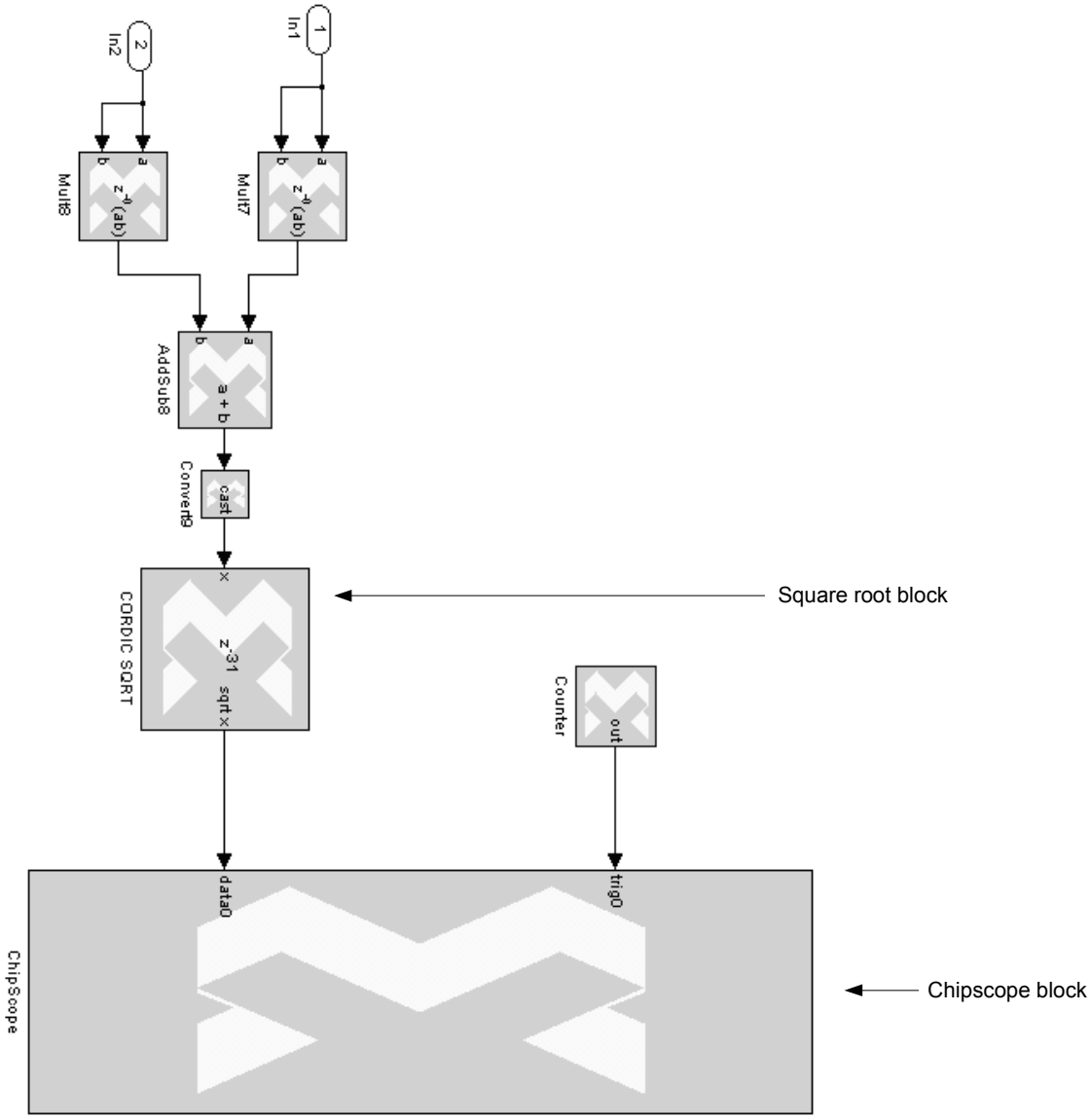
In2
In1
Mult8
Mult7
AddSub8
Convert9
CORDIC SQRT
Square root block
Counter
ChipScope
Chipscope block

REFERENCE LIST

[1] Toshiyuki Maeyama and Takashi Inoue, “Development of Cellular Repeater System with Radio Echo Suppresser,” IEICE Transactions on Communications, vol. J87-B, pp. 1194-1202, 2004.

[2] Hiroyuki Hamazumi, Koichiro Imamura Naohiko Iai, Kazuhiko Shibuya and Makoto Saski, “A Study of a Loop Interference Canceller for the Relay Stations in an SFN for Digital Terrestrial Broadcasting,” IEEE Global Telecommunications Conference, vol.1, pp. 167-171, September 2000.

[3] Christopher R. Anderson, Seshagiri Krishnamoorthy, Chris G. Ranson, Todd J. Lemon, William G. Newhall, Thomas Kummetz and Jeffery H. Reed, “Antenna Isolation, Wideband Multipath Propagation Measurements, and Interference Mitigation for On-frequency Repeaters,” IEEE Proceedings of Southeast Conference, pp. 110- 114, March 2004.

[4] Hiroshi Suzuki, Kazuhito Itoh, Yoshio Ebine and Mitsuo Sato, “A Booster Configuration with Adaptive Reduction of Transmitter-Receiver Antenna Coupling for Pager Systems,” IEEE Vehicular Technology Conference, vol.3, pp. 1516-1520, 1999.

[5] S.J. Kim, J.Y. Lee, J.C. Lee, J.H. Kim, B. Lee and N.Y. Kim, “Adaptive Feedback Interference Cancellation System (AF-ICS),” Microwave Symposium Digest, vol.1, pp. 627-630, June 2003.

[6] Jin-Kuk Lee, Sang-Keun Park, Heung-Jae Choi, Yong-Chae jeong and Jae-Hun Yun, “A Design of Co-channel Feedback Interference Cancellation System using the Analog Control,” European Microwave Conference, pp. 153-156, September 2006.

[7] Ali Hazmi, Jukka Rinne and Markku Refors, “Cancellation of Loop Interference with Exponential Profile using Autocorrelation method in

OFDM based systems," International Conference on Communications Systems, pp. 140-144, September 2004.

[8] Karim M.Nasr, John Cosmas, Maurice Bard and Jeff Gledhill, "An Echo Canceller for DVB-T/H On-Channel Repeaters," IEEE Vehicular Technology Conference, pp.639-643, April 2007.

[9] Ali H.Sayed, Fundamentals of Adaptive Filtering, Wiley, 2003.

[10] Joseph Shapira and Shumuel Y.Miller, CDMA Radio with Repeaters, Springer, 2007.

[11] John G. Proakis, Digital Communications, Fourth Edition, McGraw-Hill, 2000.

[12] Theodore Rappaport, Wireless Communications: Principles and Practice, Second Edition, Prentice Hall, 2002.

[13] Fading Channels, MATLAB (version 7.4) Communication Toolbox

[14] http://www.ericsson.com/technology/whitepapers/innovations_in_wcdma.pdf, August 2009.

[15] http://attach.baisi.net/getattach.php?a=evm_measure.pdf&b=forumid_610%2Fevm_measure_YzhetlNWJyGf.pdf&c=application%2Fpdf, August 2009.

[16] http://www.xilinx.com/support/documentation/boards_and_kits/ug_xtremedsp_devkitIV.pdf, August 2009.

[17] http://www.xilinx.com/itp/xilinx4/data/docs/cgd/entry7.html, August 2009.

[18] http://en.wikipedia.org/wiki/Gradient_descent, August 2009.